

Article

Symmetry/Asymmetry of the NHN Hydrogen Bond in Protonated 1,8-Bis(dimethylamino)naphthalene

Patrycja Piękoś¹, Aneta Jezierska^{1,*} , Jarosław J. Panek¹ , Eugene A. Goremychkin², Alexander F. Pozharskii³, Alexander S. Antonov⁴ , Peter M. Tolstoy⁴  and Aleksander Filarowski^{1,*} 

¹ Faculty of Chemistry, University of Wrocław, 14 F. Joliot-Curie str., 50-383 Wrocław, Poland; 302077@uw.edu.pl (P.P.); jaroslaw.panek@chem.uni.wroc.pl (J.J.P.)

² Frank Laboratory of Neutron Physics, Joint Institute for Nuclear Research 6 F. Joliot-Curie str., 141980 Dubna, Russia; goremychkin@jinr.ru

³ Department of Chemistry, Southern Federal University, Zorge 7, 344090 Rostov-on-Don, Russia; apozharskii@sfnu.ru

⁴ Institute of Chemistry, St. Petersburg State University, Universitetskij pr. 26, 198504 St. Petersburg, Russia; aleksandr.antonov@spbu.ru (A.S.A.); peter.tolstoy@spbu.ru (P.M.T.)

* Correspondence: aneta.jezierska@chem.uni.wroc.pl (A.J.); aleksander.filarowski@chem.uni.wroc.pl (A.F.); Tel.: +48-71-3757224 (A.J.); +48-71-3757229 (A.F.)

Received: 23 October 2020; Accepted: 20 November 2020; Published: 23 November 2020



Abstract: Experimental and theoretical results are presented based on vibrational spectra and motional dynamics of 1,8-bis(dimethylamino)naphthalene (DMAN) and its protonated forms (DMANH⁺ and the DMANH⁺ HSO₄⁻ complex). The studies of these compounds have been performed in the gas phase and solid-state. Spectroscopic investigations were carried out by infrared spectroscopy (IR), Raman, and incoherent inelastic neutron scattering (IINS) experimental methods. Density functional theory (DFT) and Car–Parrinello molecular dynamics (CPMD) methods were applied to support our experimental findings. The fundamental investigations of hydrogen bridge vibrations were accomplished on the basis of isotopic substitutions (NH → ND). Special attention was paid to the bridged proton dynamics in the DMANH⁺ complex, which was found to be affected by interactions with the HSO₄⁻ anion.

Keywords: IINS; DMAN; proton sponge; intramolecular hydrogen bond; DFT; CPMD

1. Introduction

In the last few years, considerable attention has been devoted to the symmetry of hydrogen bonding [1–10]. Hydrogen maleate, hydrogen phthalate anions, and proton sponges have been studied intensively due to their physicochemical features that are derived from the presence of an intramolecular hydrogen bond [2,4,5,7,8,11–14]. The significance of proton sponges, the main object of the current study, is demonstrated by their high presence in the literature (e.g., [15–21]). The discussion concerning the symmetry of the hydrogen bridge has been the subject of many experimental and theoretical studies. The X-ray, neutron diffraction, incoherent inelastic neutron scattering (IINS), infrared spectroscopy (IR), and nuclear magnetic resonance (NMR) methods of Limbach et al. [22–25] and Perrin et al. [1,7] have been applied to investigate the isotopic perturbation of the equilibrium [26] to distinguish between symmetric and asymmetric intramolecular hydrogen bonds.

Starting with the paper by Alder [27], where the first synthesis of 1,8-bis(dimethylamino)naphthalene (DMAN; naphthalene proton sponges) was published, proton sponges have raised a great interest on the side of researchers [28–33]. The most promising feature of

proton sponges is their significant basicity, which has been investigated in a series of papers [34–39]. The next unique trait of proton sponges is their extremely strong hydrogen bonding, already analyzed by structural and spectroscopic methods [40–50]. Remarkably, the protonation process can occur by the direct proton transfer from a strong acid to between two nitrogen atoms. However, in [51–54], an elaborate out-in protonation mechanism is outlined. Such rotational mechanism rests upon the intermolecular protonation of one of the amino groups by a strong acid, with the following reorientation (isomerization) of this group, and formation of the intramolecular hydrogen bond NHN. The scientific value/attractiveness of proton sponges also lies in the possibility of double protonation of the hydrogen bridge [37,55].

The localization of the proton in a very short hydrogen bridge in proton sponges seems to be a very interesting scientific challenge. A solution to such a challenge has been suggested in a number of structural as well as spectroscopic studies [38–45]. Theoretical studies of proton dynamics in a hydrogen bridge are of particular interest [55–61] because they provide information on the time-evolution of metric parameters involved in hydrogen bridge formation, therefore giving an insight into the dynamical features of the studied system. It is very hard to get similar information only by the construction and analysis of standard/static models. These papers show the dynamics of the bridged proton in proton sponges by the Car–Parrinello molecular dynamics (CPMD) method. In [62–67], the authors investigated a strong influence of steric squeezing of bulky groups in Positions 2 and 7 on the hydrogen bridge in proton sponges. In the recent paper by Pozharskii et al. [68], the authors opened up a synthetic route to new proton sponges, exhibiting the strong buttressing effect mentioned above. The expected result, which is currently being verified experimentally, is an extremely low energy barrier on proton transfer ($\Delta E \sim 0.1$ kcal/mol, which effectively means the barrier's absence) in these new proton sponges, which are also expected to possess extremely short NHN bridges [68].

It should be noted that proton sponges are interesting not only in the area of fundamental research. Studies have shown the potential use of the investigated proton sponges in cardiology and dye fields [69,70].

The main aim of this study is the experimental and computational investigation of the symmetry/asymmetry of the NHN hydrogen bridge in proton sponges (Figure 1). This requires a detailed structural and spectroscopic insight into hydrogen bridge properties. For this purpose, the paper presents two synthesized complexes—DMANH⁺ HSO₄[−] and DMAND⁺ DSO₄[−]—for the consequent studies of the isotopic effects on spectral parameters. As a part of these studies, IINS and IR spectra have been measured in the wide spectral range of the synthesized complexes. Here, for the first time, we present the IINS results for the discussed complex and their comparison with data obtained by Car–Parrinello molecular dynamics [71]. The analysis of the experimental and calculated vibrational spectra was completed; the studies of the bridged proton dynamics and molecular skeleton symmetry were performed using the Car–Parrinello molecular dynamics (CPMD) method [71].

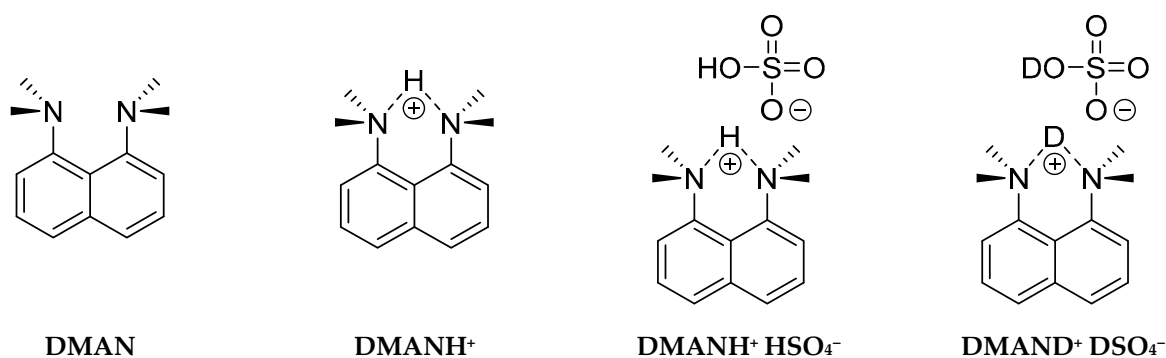


Figure 1. Chemical structures of studied molecules DMAN and DMANH⁺ and complexes DMANH⁺ HSO₄[−] and DMAND⁺ DSO₄[−].

2. Materials and Methods

2.1. Compound and Synthesis

The studied compound and solvents were purchased from Sigma-Aldrich and used without further purification. Melting points were determined in glass capillaries on a Stuart SMP30 device and are uncorrected.

Bis(dimethylamino)naphthalene Sulfate

To the vigorously stirred solution of 1,8-bis(dimethylamino)naphthalene (10 g, 47 mmol) in 200 mL of diethyl ether, a 98% aqueous solution of H₂SO₄ (2.7 mL, 50 mmol) was added dropwise. The resulting suspension was additionally stirred for 15 min and filtrated. The precipitate was dried over P₂O₅ in vacuo (2 torr) for 2 h to turn the product into white crystalline powder with a 90% yield (13.2 g); melting point (mp) 177–178 °C. ¹H NMR (400 MHz, DMSO-*d*₆) δ 18.30 (s, 1H), 8.15–8.07 (m, 4H), 7.74 (t, *J* = 7.9 Hz, 2H), 3.15 (d, *J* = 2.6 Hz, 12H). ¹³C NMR (100 MHz, DMSO-*d*₆) δ 145.17, 135.29, 129.33, 127.43, 122.29, 119.45, 46.23.

8-Bis(dimethylamino)naphthalene Sulfate-*d*₂

To the vigorously stirred solution of 1,8-bis(dimethylamino)naphthalene (10 g, 47 mmol) in 200 mL of absolute diethyl ether, a 98% solution of D₂SO₄ in D₂O (2.8 mL, 50 mmol) was added dropwise. The resulting suspension was additionally stirred for 15 min and filtrated. The precipitate was dried over P₂O₅ in vacuo (2 torr) for 2 h to turn the product into white crystalline powder with a 95% yield (14 g); mp 178–179 °C. ¹H NMR (400 MHz, D₂O) δ 7.84–7.74 (m, 4H), 7.55 (t, *J* = 8.0 Hz, 2H), 3.00 (s, 12H). ¹³C NMR (100 MHz, D₂O) δ 143.79, 135.04, 129.08, 126.89, 121.20, 118.63, 45.58. ²H NMR (500 MHz, solid-state) δ 19.47, 14.20. The solid-state magic angle spinning (MAS) ²H NMR (76.7 MHz, 18 kHz spinning, 3.2 mm rotor) confirmed the successful deuteration: two isotropic signals were observed at ca. 19.5 ppm (the NDN bridging deuterons) and ca. 14.2 ppm (the remaining DSO₄[−] deuterons; see Figure A8).

2.2. Infrared Spectra Measurements

Fourier transform far- and middle-infrared (FT-FIR and FT-MIR) absorption measurements were performed using a Bruker Vertex 70v vacuum Fourier transform spectrometer. The transmission spectra were collected with a resolution of 2 cm^{−1} with 64 scans. The FT-FIR spectra (500–50 cm^{−1}) were collected for the samples suspended in Apiezon N grease and placed on a polyethylene disc. The FT-MIR spectra were collected for the samples in a KBr pellet.

2.3. Incoherent Inelastic Neutron Scattering (IINS) Measurements

Inelastic neutron scattering spectra were measured using the time-of-flight inverted geometry spectrometer NERA (pulsed IBR-2 reactor in JINR (Dubna, Russia)) at 5 K temperature in the 5–1600 cm^{−1} spectral region. The spectra were converted from neutron per channel to S(**Q**, ω) function per energy transfer according to the scattering law [72].

The IINS and IR spectra of DMAN are presented in Figure A1.

2.4. NMR Measurements

Liquid-state NMR experiments were performed using a Bruker Avance III 400 spectrometer (400.13 MHz for ¹H and 100.61 MHz for ¹³C) at the Centre for Magnetic Resonance, St. Petersburg State University Research Park. ¹H and ¹³C NMR chemical shifts were referenced to tetramethylsilane (TMS) using the unified scale, according to IUPAC recommendations [73]. The number of scans varied between 128 and 256. The corresponding spectra are presented in Figures A2–A8. The NMR spectra and the line shape analysis were performed using MestReNova 8.1 software [74].

2.5. Static DFT and D3-DFT Calculations

The static density functional theory (DFT) calculations were accomplished for DMANH⁺ and the DMANH⁺ HSO₄⁻ complex using the Gaussian 16 Rev. C01 program [75], with the correlation of the Lee–Yang–Parr formula (B3LYP) [76,77]. The 6-311++G(d,p) basis set [78–80] was used. The atom pair-wise correction method for dispersion forces (DFT-D3) was applied [81]. The potential curves of proton transfer within the NHN intramolecular hydrogen bond were calculated using the stepwise elongation of the N–H distance by 0.05 Å gradient, with full optimization of the rest of the structural parameters. The calculations were performed for the gas phase and acetonitrile (ACN; the polarizable continuum model (PCM) approach [82] in an IEF-PCM formulation). The computed structures were shown using the MOLDEN program [83].

2.6. Symmetry-Adapted Perturbation Theory Calculations

Next, the investigation of the interaction energy components in the DMANH⁺ HSO₄⁻ complex was carried out within the framework of symmetry-adapted perturbation theory (SAPT) [84]. The simulations were performed at the SAPT2 level of theory [85] for the B3LYP/6-311++G(d,p) structure. The SAPT2 calculations for the DFT-optimized structures were carried out with the aug-cc-pVDZ basis set [86], employed for atomic orbital expansion. The interaction energy calculated at the SAPT2/aug-cc-pVDZ level was corrected for the basis set superposition error using the counterpoise approach, taking DMANH⁺ as the “monomer” and the HSO₄⁻ anion as the second “monomer” of the “dimer”. The SAPT calculations were performed using the Psi4 1.2.1 [87] program.

2.7. Car–Parrinello Molecular Dynamics Simulations

The first-principle molecular dynamics (FPMD) simulations were performed on the basis of the Car–Parrinello method [71]. The DMAN molecule and its protonated complex with HSO₄⁻ were investigated in the gas phase. The models for CPMD simulations were constructed based on DFT results for DMAN and the DMANH⁺ HSO₄⁻ complex. The computations were carried out using the CPMD 3.17.1 program [88]. Molecular dynamics trajectory postprocessing was achieved with the utilities developed onsite and with the VMD 1.9.3. program [89]. The Gnuplot graphics package [90] and the VMD 1.9.3. program [89] were used for the results’ graphical presentation. The DMAN molecule and its protonated complex were placed in cubic boxes with $a = 16$ Å and $a = 18$ Å, respectively. The weak interactions present in the investigated complex were reproduced with the empirical van der Waals protocol developed by Grimme [81]. The PBE exchange-correlation DFT functional [91] was used in both simulations. The Troullier–Martins norm-conserving pseudopotentials [92] substituted the core electrons, while the plane-wave Kohn–Sham orbitals were set to possess the maximum kinetic energy value of 80 Ry for DMAN and 100 Ry for the DMANH⁺ HSO₄⁻ complex. Hockney’s scheme of periodicity removal [93] ensured the simulation in the regime of the isolated system. The translational and rotational movements of the molecules, resulting from numerical rounding errors, were also removed at every 20 MD steps during the simulations. The dynamics of the orbital coefficients were carried out with the fictitious orbital mass of 400 a.u., and the timestep of the nuclear dynamics was 3 a.u. in the case of DMAN and 2 a.u. in the case of the studied complex. The CPMD simulations were performed with the equilibration of the simulation conditions and the subsequent trajectory collection for further metric and spectroscopic feature analyses. Equilibration was carried out by thermostating the ionic temperature at 300 K for DMAN and 297 K for the complex using a separate Nosé–Hoover thermostat chain, with default settings for each degree of freedom (“massive” thermostating) [94,95]. The data collection lasted for 21.8 ps for DMAN and 24.1 ps for the DMANH⁺ HSO₄⁻ complex. The NVE microcanonical ensemble was used, i.e., the thermostating was discontinued during the production run simulations. Then, the obtained trajectories were used to extract information on the time-evolution of atoms forming the hydrogen bridge and of other metric parameters, e.g., the NC–NC dihedral angle, as well as to determine the vibrational features from the power spectra of the atomic velocity of the investigated molecules (Figures A9 and A10).

3. Results and Discussion

3.1. SAPT Analysis of the $\text{DMANH}^+ \text{HSO}_4^-$ Complex

The SAPT scheme partitions the interaction energy of a dimer into diverse components [84,85]. For the purpose of this study, however, it is sufficient to use the most general scheme of grouping these components into electrostatic, exchange, polarization, and dispersion terms. The first one refers to the Coulombic interaction between the nuclei and electronic densities of the monomers DMANH^+ and HSO_4^- , with the assumption that these monomers are in their original electronic states, that is, DMANH^+ is not perturbed by HSO_4^- and vice versa. The same assumption holds for the exchange (Pauli repulsion) term. The effects of mutual polarization or induction, together with their impact on Pauli repulsion, are included in the third term. Finally, the last component gathers the instantaneous multipole attraction (dispersion forces) between the monomers. These four terms are composed of many contributions, some of them arising as the result of intramonomer electron correlation. Selecting the noncorrelated terms yields the Hartree–Fock interaction energy. All these contributions for the $\text{DMANH}^+ \text{HSO}_4^-$ complex are summarized in Table 1.

Table 1. Interaction energy components (in kcal/mol) calculated at the SAPT2/aug-cc-pVDZ level of theory for the B3LYP/6-311++G(d,p) structure of the $\text{DMANH}^+ \text{HSO}_4^-$ complex in a vacuum.

Electrostatics	Exchange	Induction	Dispersion	Total HF	Total SAPT2
−87.17	24.98	−14.64	−11.44	−79.25	−88.28

A striking agreement is found between the electrostatics term and total SAPT2 interaction energy. The remaining three components of the intermolecular forces are close to zero when summed up. This fact is the manifestation of the dominant role of electrostatics in an ionic complex. Exchange, induction, and dispersion are important individually, but their combined effect is just one kcal/mol of destabilization. Interestingly, even for such a strongly bound complex, electron correlation strengthens the interaction by 9 kcal/mol, almost 10% of total SAPT2 energy. Nevertheless, the net interaction strength corresponds strongly to the purely Coulombic picture of the cation–anion pair. The impact of this strong electrostatic interaction is visible in the modified time scale of bridge proton dynamics, which is described in the next section.

3.2. Metric Parameter Time-Evolution Analysis Based on Car–Parrinello Molecular Dynamics

The CPMD simulations in the gas phase were carried out by us with a twofold aim: first, to identify the apparent symmetry of the gas-phase DMAN molecular skeleton, and second, to investigate in detail the behavior of the intramolecular hydrogen bridge. The timescale of over 20 ps was found sufficient to cover the characteristic features of the neutral and protonated DMAN. Firstly, we examined the relative arrangement of the aromatic rings, distorted by the sterically bulky substituents of the amine moieties. Figure 2 presents the time evolution of the relevant CN–CN dihedral angle between the C–N bonds (which effectively measures whether the two naphthalene rings are coplanar).

The relatively slow motion of the aromatic rings is rather strongly harmonic in the nonprotonated DMAN, but the symmetry of the molecular skeleton is broken by the methyl groups, which are bulky enough to prevent the two rings from being coplanar. The average CN–CN dihedral angle is, for this case, 152.1°. When the $\text{DMANH}^+ \text{HSO}_4^-$ complex is studied, the average angle is 181.2°, much closer to the “ideal coplanarity” value. These findings are determined by the fact that in the nonprotonated DMAN, the lone pairs of the nitrogen atoms act, in addition to the size of the $\text{N}(\text{CH}_3)_2$ groups, as additional “steric-blocking” factors, and they do not allow the substituents of the naphthalene ring to cross the molecular plane. In effect, the movement of the $-\text{N}(\text{CH}_3)_2$ moieties is limited in its amplitude and centered at a value far from 180°. Additionally, the $\text{N}\cdots\text{N}$ distance is also larger in DMAN than in the protonated complex. This brings us to the role of the proton in the NHN hydrogen bridge.

The proton connects the $-N(CH_3)_2$ moieties closely, bringing about a decrease in the $N\cdots N$ distance and increasing in the planarity of the compound. Additionally, the HSO_4^- group cannot be neglected while analyzing the results. The intermolecular dynamics of the $DMANH^+ HSO_4^-$ moieties are very slow in comparison to the intramolecular vibrations, leading to larger and less systematic amplitudes of the dihedral angle seen in Figure 2. Thus, within the 20 ps time scale, one might conclude that the cationic $DMANH^+$, with the hydrogen bridge intramolecular linker, is planar but not necessarily more harmonic. It is visible that the trajectory of the dihedral angle is very harmonic for $DMAN$ but much more rugged for $DMANH^+$. This suggests that the dynamics of the hydrogen bridge in the complex might reveal strong anharmonicity (see Figure 3).

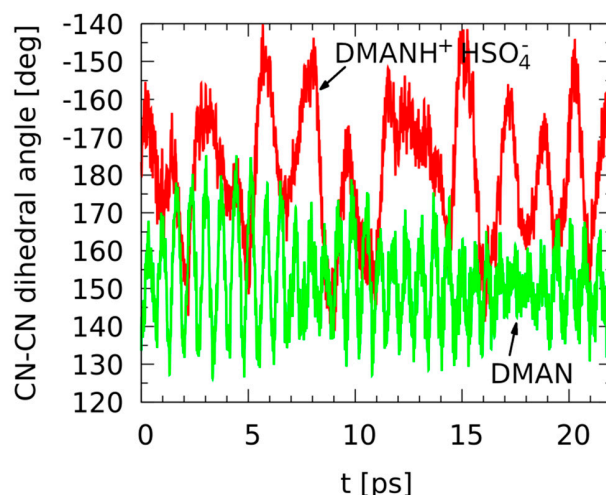


Figure 2. Time evolution of the dihedral angle between the C-N bonds—results of the gas-phase Car–Parrinello molecular dynamics (CPMD) simulations for the neutral $DMAN$ (green line) and $DMANH^+ HSO_4^-$ (red line).

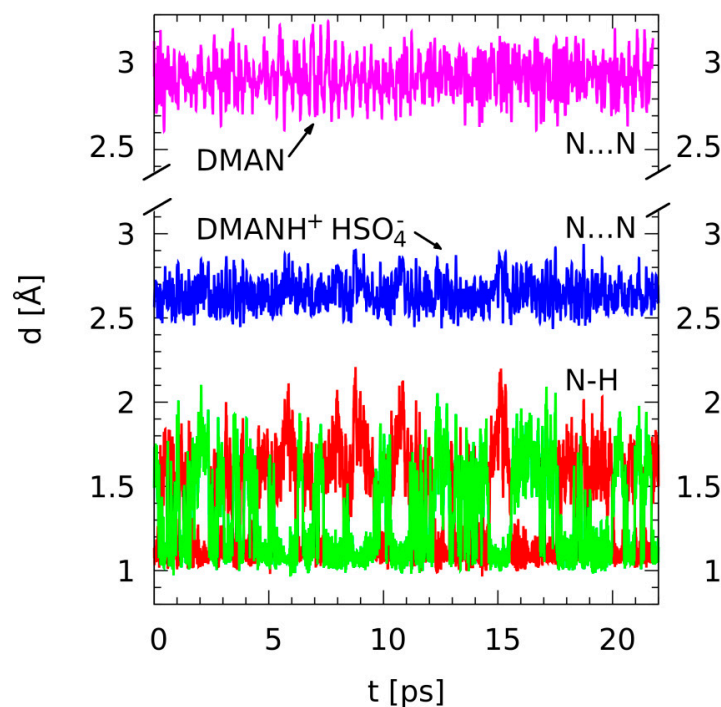


Figure 3. Time evolution of selected metric parameters—results of the gas-phase CPMD simulations for the neutral $DMAN$ (purple line: $N\cdots N$ distance) and $DMANH^+ HSO_4^-$ (blue line: $N\cdots N$ distance; red and green lines: bridge $N-H$ distances).

Figure 3 is an example of the proton bridge dynamics studied by first-principle molecular dynamics methods. Time evolution of the important metric parameters (N-H, H...N, and N...N distances) is presented. The time scale available for the CPMD simulation is such that we could observe the high mobility of the bridged proton; the proton moves between the donor and acceptor atoms, which is indicated by the red and green lines crossing continually. For clarity, the data for the nonprotonated DMAN (the N...N distance) is presented as the inset above the data for the protonated complex. Figure 3 shows clearly how strongly the bridged proton is able to force the two nitrogen atoms closer. The N...N distance averaged over the CPMD run is 2.929 Å for the neutral DMAN and only 2.646 Å for the DMAN HSO₄⁻ complex. The hydrogen bridge is not totally symmetric within the 20 ps time scale: the averages of the two N-H distances are 1.346 and 1.396 Å. We do not expect this lack of symmetry in the bridge to result from any significant physical phenomenon because the molecular structure of DMANH⁺ does not contain any substituents that could break the symmetry of the proton potential function. We attribute the imperfect averaging of two N-H distances to the effect of the slow motion of the heavier HSO₄⁻ anion in the neighborhood of the hydrogen bond. It is visible that the proton resides at a given nitrogen atom for a period of ca. 1 picosecond, and then it abruptly switches to the other nitrogen site. This residence period of ca. 1 picosecond is much longer than the time of 0.3 ps that was observed in the CPMD simulations of gas-phase DMANH⁺ [56]. SAPT analysis has shown the absolutely dominant role of the electrostatic interactions, and this fact means that the structures with localized charges are preferred. In turn, this means that the transfer of the bridged proton over the hydrogen bond center displaces the location of the positive charge and is accompanied by the motion of the heavier HSO₄⁻ anion as well. Moreover, the central-symmetric structures with two equal N-H distances are not favored because such a structure would have the most symmetric charge distribution and would provide less than optimal electrostatic interaction.

3.3. DFT and D3-DFT Analysis of PES

Part of the presented studies covers the investigation of the potential curves of the proton transfer in DMANH⁺ and DMANH⁺ HSO₄⁻. The studies are based on the calculations of the potential curves by the B3LYP/611++G(d,p) method, with Grimme correction (D3-DFT) [81] and without it (DFT), for the gas phase and involve the influence of the solvent (acetonitrile; the PCM model). The calculations with Grimme correction exposed a lower potential barrier of the proton transfer in the studied molecules in the gas phase and in the polar medium (Figure 4A,B) than the calculation without this correction. This conclusion is absolutely reliable since it is in accordance with the approximation suggested by Grimme [96]. Taking into account that dispersive interactions must show a stronger interrelation in the hydrogen bridge, as a consequence, there is a decrease of the potential barrier.

The analysis of the influence of the polar environment (the transition from the gas phase to acetonitrile) reveals the difference between DMANH⁺ and DMANH⁺ HSO₄⁻. Notably, the specific interactions (intermolecular hydrogen bond between DMANH⁺ and HSO₄⁻) increase the value of the potential barrier for the proton transfer in the intramolecular hydrogen bridge due to its weakening by bifurcation. In the case of DMANH⁺, the growth of environment polarity also brings about the increase of the barrier for proton transfer. This result, obtained by DFT and D3-DFT calculations, proves that the polarity increase leads to the weakening of the symmetric NHN hydrogen-bonding in DMANH⁺ under the absence of outside specific interactions (HSO₄⁻). This trend is consistent with the generally accepted concepts of hydrogen bonds presented in [97,98]. Nevertheless, reverse dependence is observed in the presence of such specific interactions. For the complex DMANH⁺ HSO₄⁻, the growth of the polar environment evokes the decrease of the barrier for the proton transfer. It is important to note that the calculation of the complex DMANH⁺ HSO₄⁻ for the gas phase does not present symmetric potential, which seemed to be expected because of the reorientation of the HSO₄⁻ anion under the proton transfer in the NHN bridge. However, the calculation of the complex DMANH⁺ HSO₄⁻ involving solvent influence has potential, with two minima of equal depth (Figure 4B).

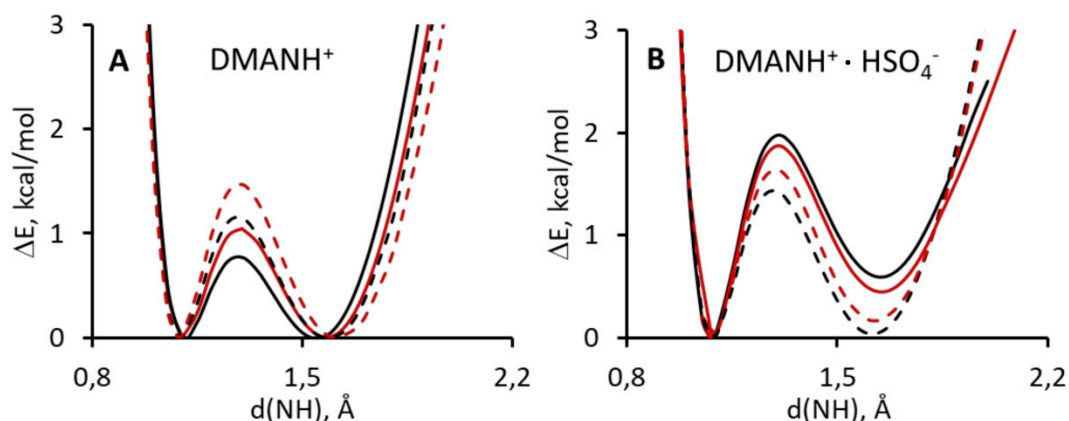


Figure 4. Calculated density functional theory (DFT) and atom pair-wise correction method for dispersion force (DFT-D3) potential energy functions for gradual proton displacement in the intramolecular hydrogen bond of DMANH⁺ (A) and DMANH⁺ HSO₄[−] (B). Left panel: black solid line, DMANH⁺ with Grimme approach for gas phase; red solid line, DMANH⁺ for gas phase; black dashed line, DMANH⁺ with Grimme approach for ACN; red dashed line, DMANH⁺ ACN. Right panel: black solid line, DMANH⁺ HSO₄[−] with Grimme approach for gas phase; red solid line, DMANH⁺ HSO₄[−] for gas phase; black dashed line, DMANH⁺ HSO₄[−] with Grimme approach for ACN; red dashed line, DMANH⁺ HSO₄[−] for ACN.

The whole picture of the calculated potential curves enables us to conclude that the hydrogen bonding in DMANH⁺ HSO₄[−] is symmetric but with the height of the barrier for proton transfer equal to 1.5 kcal/mol.

3.4. Comparison of Experimental IINS, IR, and Calculated CPMD Spectra

The spectroscopic measurements and theoretical calculations of molecular properties are complementary tools to gain insight into the nature of the studied systems. In particular, static DFT and dynamical CPMD simulations have determined the symmetry/asymmetry of the proton potential function in the bridge. There are, however, some points in which the experiment and calculations can be directly conjugated. Thus, this part of the paper is concerned with the analysis of the spectral bands assigned to the vibrations of bridged proton and methyl groups, performed by means of CPMD and DFT calculations (Figures 5 and 6, Tables A1 and A2). Moreover, these studies verify the reliability of the CPMD simulations. As well-known [99–103], in IINS spectra, the most intensive are the vibration bands of hydrogen atoms, especially torsional vibrations of the methyl groups [102–110]. Therefore, we conducted the measurements of IINS spectra and the calculation of the vibrations of all the hydrogen atoms of the investigated DMAN complex by the CPMD method (Figures A9 and A10). According to the performed CPMD calculations, the bands of the deformational and torsional vibrations are located at 1380, 1100, 1030, 970, and 230 cm^{−1}. Notably, the CPMD calculation gives a picture of more expanded bands, which is closer to reality (see spectra and Figures 5A and 6C,D). There is a very good agreement between the calculated vibrations of the methyl groups and the measured positions of the bands in the IINS spectrum <1300 cm^{−1} (red arrows on Figure 5). The bands at 1380, 1100, 1030, and 970 cm^{−1} are assigned to δ , γ deformational, and τ torsional vibrations of the methyl groups, respectively. Interestingly, only the IINS spectrum features all the mentioned bands; meanwhile, IR and Raman spectra are characterized by just two bands (1050 and 330 cm^{−1}). This fact clearly points out the prevalence of the IINS method over traditional IR and Raman methods when it comes to the studies of the methyl group vibrations.

As for the analysis of the bridged proton (NHN) vibrations, the CPMD calculation revealed the presence of only one wide intensive band covering a spectral region of 1000–2500 cm^{−1} and centered at 1500 cm^{−1} (Figure 6C). This calculated band corresponds to the wide band of a weak intensity in the Raman spectrum (Figure 6B). A weak intensity of the bands in the Raman spectrum, assigned

to the hydrogen bridge vibrations, is quite reasonable and complies with the commonly accepted rule [111,112]. However, in the infrared spectrum of the studied complex (Figure 6A), one can observe a wide band (300–3000 cm^{-1}) called Zundel's continuum absorption, which is an indicator of extra strong hydrogen bonds [113,114]. The CPMD calculation, which complies with the experimental IR data, states that 3500, 1100–1000, and 300–80 cm^{-1} bands correspond to hydroxyl group vibrations (corresponding, respectively, to the $\nu(\text{OH})$, $\delta(\text{OH})$, $\gamma(\text{OH})$, and $\tau(\text{OH})$ modes).

For a more precise analysis of the bands in the IINS spectra of the studied complex, we have also completed the studies of its deuterio-substituted derivative ($\text{NHN} \rightarrow \text{NDN}$). The degree and reliability of the synthesized deuterio-substituted complex are presented by means of NMR measurements (Figures A5–A8). The comparison of two IINS spectra of the protonated and deuterated complexes (Figure A11) showed a decrease of the band intensity at 530 and 262 cm^{-1} . These bands are assigned to the NHN and NHO vibrations of the hydrogen bridges. A similar interpretation was earlier performed in [115,116].

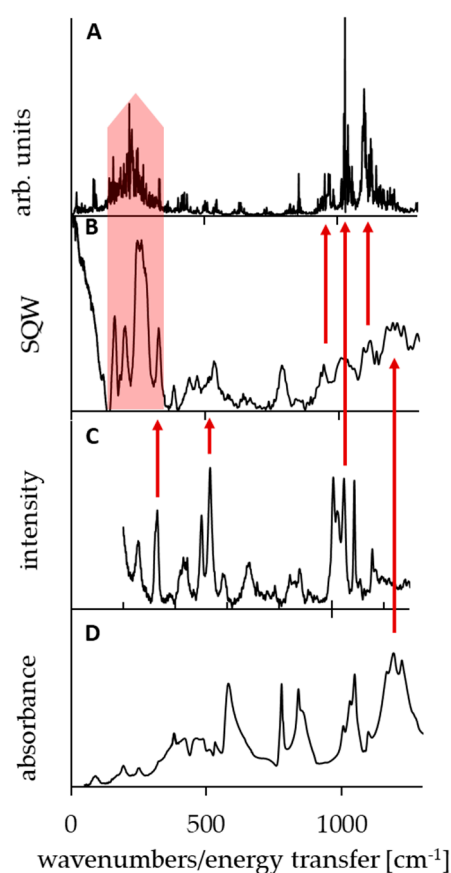


Figure 5. Simulated power spectrum of the torsional methyl group modes by the CPMD method (panel (A)) and experimental incoherent inelastic neutron scattering (IINS; panel (B)), Raman (panel (C)), and infrared spectroscopy (IR) spectra (panel (D)) of $\text{DMANH}^+ \text{HSO}_4^-$. The red arrows show the best fit between the calculated and experimental bands.

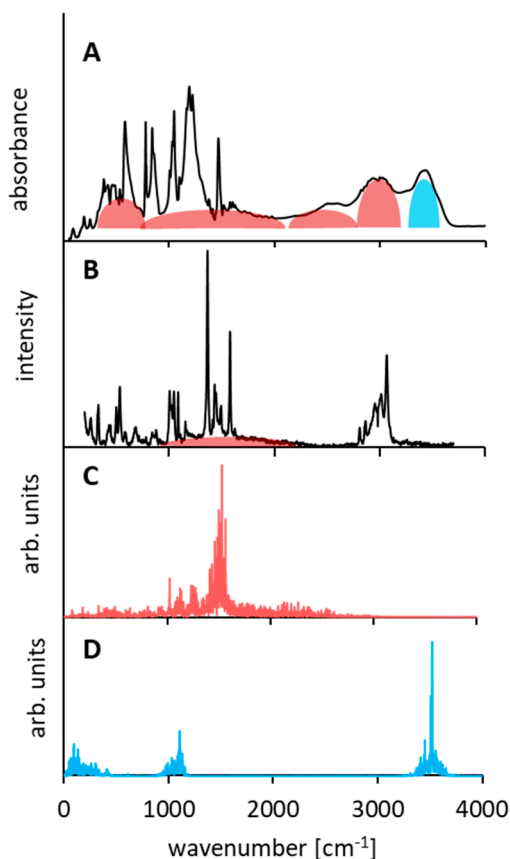


Figure 6. Experimental IR (panel (A)), Raman (panel (B)) and atomic velocity power spectra for the hydrogen-bonded protons of the $\text{DMANH}^+ \text{HSO}_4^-$ complex (results of the CPMD simulation in the gas phase; panels (C) and (D) for NHN and OH protons, respectively).

4. Conclusions

In this study, we present the experimental investigation of 1,8-bis(dimethylamino)naphthalene sulfate ($\text{DMANH}^+ \text{HSO}_4^-$, as well as its deuterated isotopolog $\text{DMAND}^+ \text{DSO}_4^-$; protonated proton sponges) in solid-state by means of inelastic incoherent neutron scattering (IINS), IR, and Raman spectroscopy, supplemented by the theoretical investigation of isolated DMANH^+ and ($\text{DMANH}^+ \text{HSO}_4^-$) salt using DFT, D3-DFT, and CPMD methods.

We show that the strong intramolecular NHN hydrogen bond in DMANH^+ moiety is asymmetric and that the bridged proton is moving in a double-well potential. However, the energy barrier for the proton transfer is very low, ca. 1.5 kcal/mol, which determines the short residence time of the proton close to one of the nitrogen atoms of about 1 ps or 0.3 ps (depending on whether the presence of the HSO_4^- anion and its motion are taken into account or not). The HSO_4^- anion interacts with the cation by forming additional intermolecular $\text{OH}\cdots\text{N}$ hydrogen bonds and occasionally by forming bifurcated hydrogen bonds with the NHN proton; nevertheless, the energy of the anion–cation interaction remains predominantly electrostatic.

We show that the polarity of the surrounding medium has an effect on the proton transfer barrier height: for isolated DMANH^+ , higher polarity increases the barrier (as it destabilizes the central-symmetric structure with the most delocalized positive charge); in contrast, for $\text{DMANH}^+ \text{HSO}_4^-$, higher polarity decreases the barrier height because of the higher stabilization of the more isolated HSO_4^- anion in the central-symmetric transition state structure.

The shortness of the NHN bridge leads to the extreme broadening of the NH stretching band in vibrational spectra (a Zundel continuum covering the 300–3000 cm^{-1} range is observed in the IR spectra). Thus, the intramolecular hydrogen bond in DMANH^+ could be classified as a low-barrier

hydrogen bond (LBHB) or a short strong hydrogen bond (SSHB), but its symmetry is present only on average. In the majority of instances, the symmetry is broken due to the asymmetric placement of the anion, whose motion determines the dynamics and drives the bridged proton transfer.

In conclusion, it is worth emphasizing that the CPMD calculation can quite realistically describe some aspects of experimental neutron scattering spectra.

Author Contributions: Conceptualization, A.J. and A.F.; methodology, P.P., A.J., J.J.P., E.A.G., A.F.P., A.S.A., P.M.T., and A.F.; software, P.P., A.J., J.J.P., E.A.G., A.F.P., A.S.A., P.M.T., and A.F.; validation, P.P., A.J., J.J.P., E.A.G., A.F.P., A.S.A., P.M.T., and A.F.; formal analysis, P.P., A.J., J.J.P., E.A.G., A.F.P., A.S.A., P.M.T., and A.F.; investigation, P.P., A.J., J.J.P., E.A.G., A.F.P., A.S.A., P.M.T., and A.F.; resources, P.P., A.J., J.J.P., E.A.G., A.F.P., A.S.A., P.M.T., and A.F.; data curation, P.P., A.J., J.J.P., E.A.G., A.F.P., A.S.A., P.M.T., and A.F.; writing—original draft preparation, A.J., J.P., and A.F.; writing—review and editing, P.P., A.J., J.J.P., E.A.G., A.F.P., A.S.A., P.M.T., and A.F.; visualization, P.P., A.J., J.J.P., E.A.G., A.F.P., A.S.A., P.M.T., and A.F.; supervision, A.J. and A.F.; project administration, A.J. and A.F.; funding acquisition, A.J. All authors have read and agreed to the published version of the manuscript.

Funding: This research was funded by the Russian Science Foundation (RSF; grant no. 18-13-00050) and the Polish Government Plenipotentiary for JINR in Dubna (75/24/2020; p. 75; data 03.02.2020).

Acknowledgments: The authors gratefully acknowledge the Wrocław Center for Networking and Supercomputing (WCSS) for generous grants of CPU time and technical support.

Conflicts of Interest: The authors declare no conflict of interest.

Appendix A

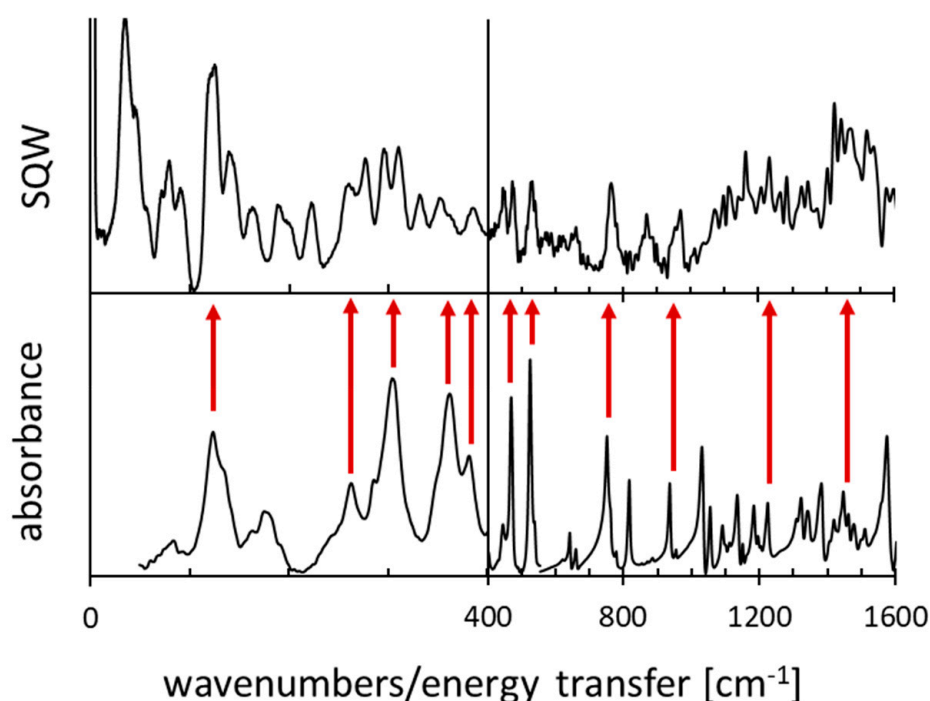


Figure A1. The IINS and IR spectra for 1,8-bis(dimethylamino)naphthalene.

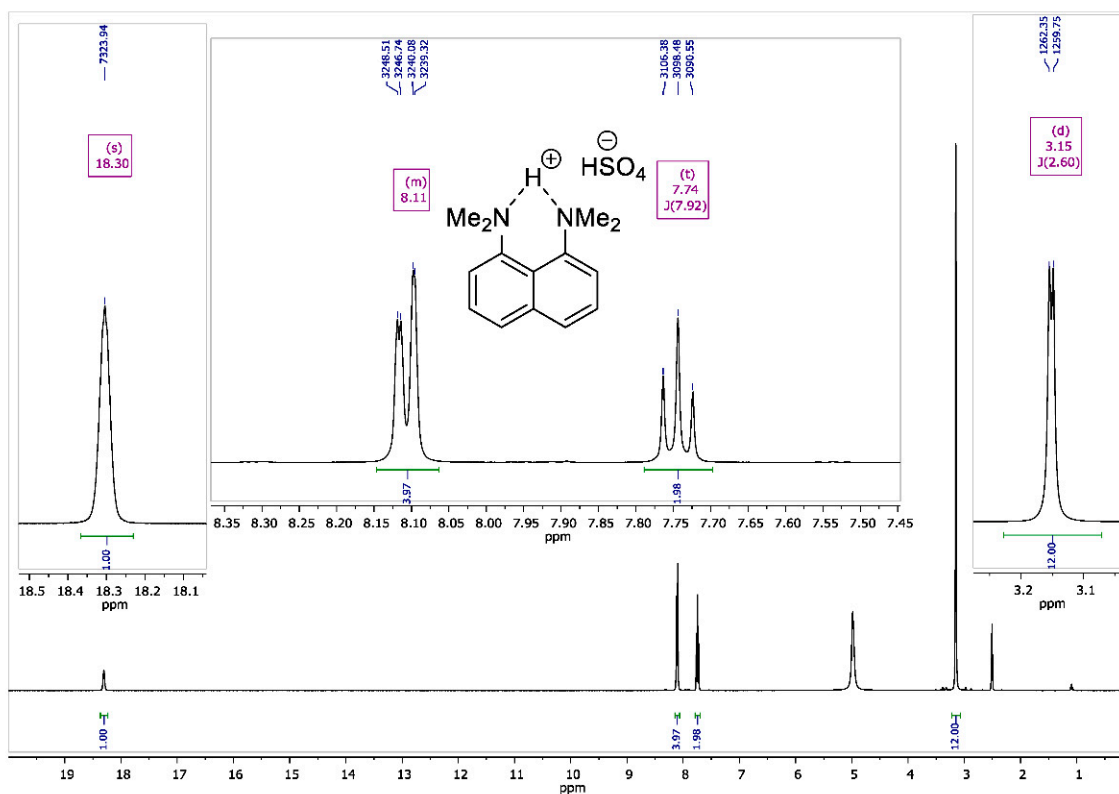


Figure A2. ^1H NMR spectrum for 1,8-bis(dimethylamino)naphthalene sulfate (400 MHz, $\text{DMSO-}d_6$).

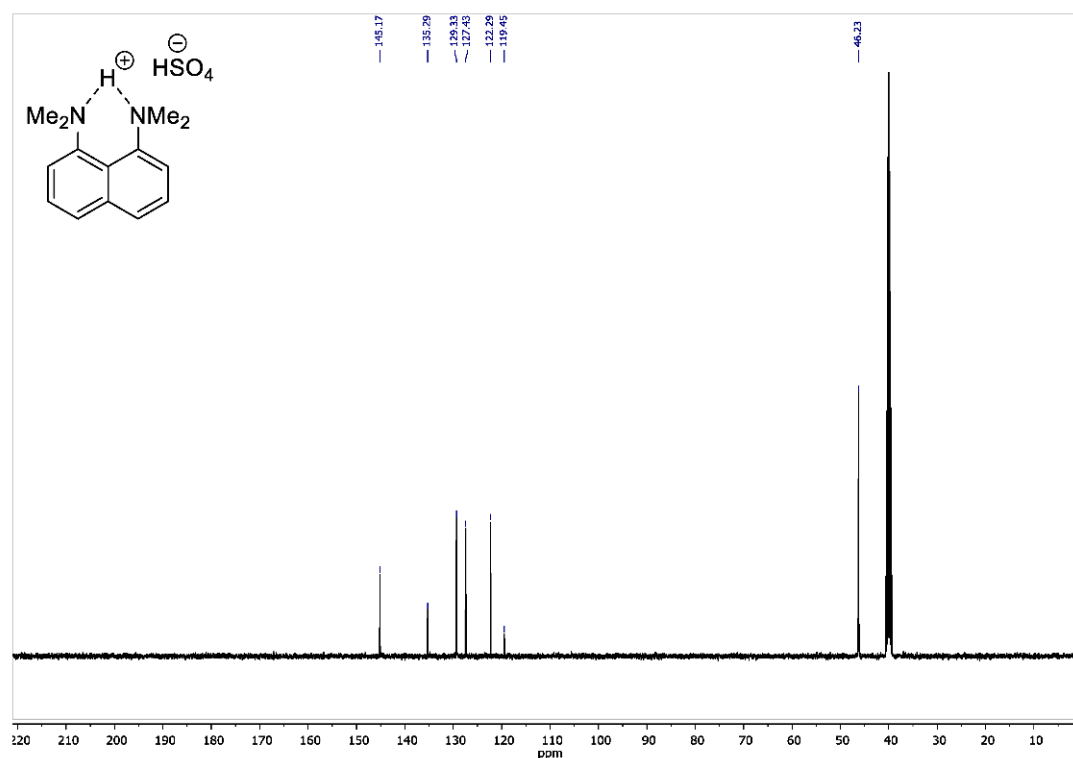


Figure A3. ^{13}C NMR spectrum for 1,8-bis(dimethylamino)naphthalene sulfate (100 MHz, $\text{DMSO-}d_6$).

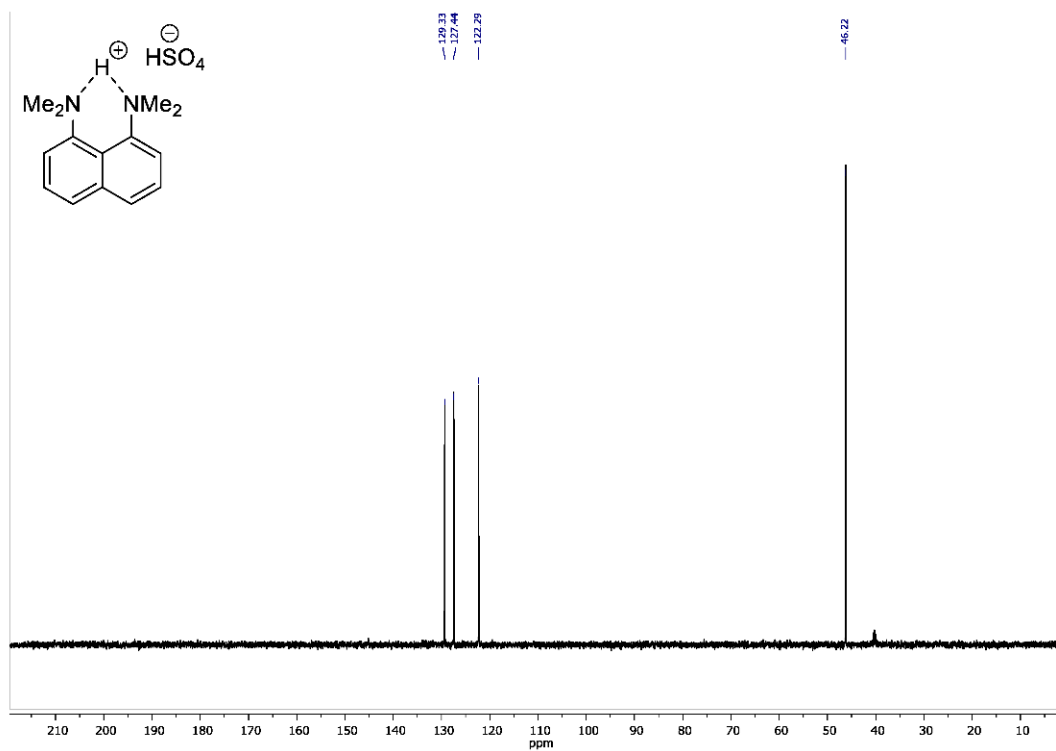


Figure A4. ^{13}C DEPT135 NMR spectrum for 1,8-bis(dimethylamino)naphthalene sulfate (100 MHz, $\text{DMSO-}d_6$).

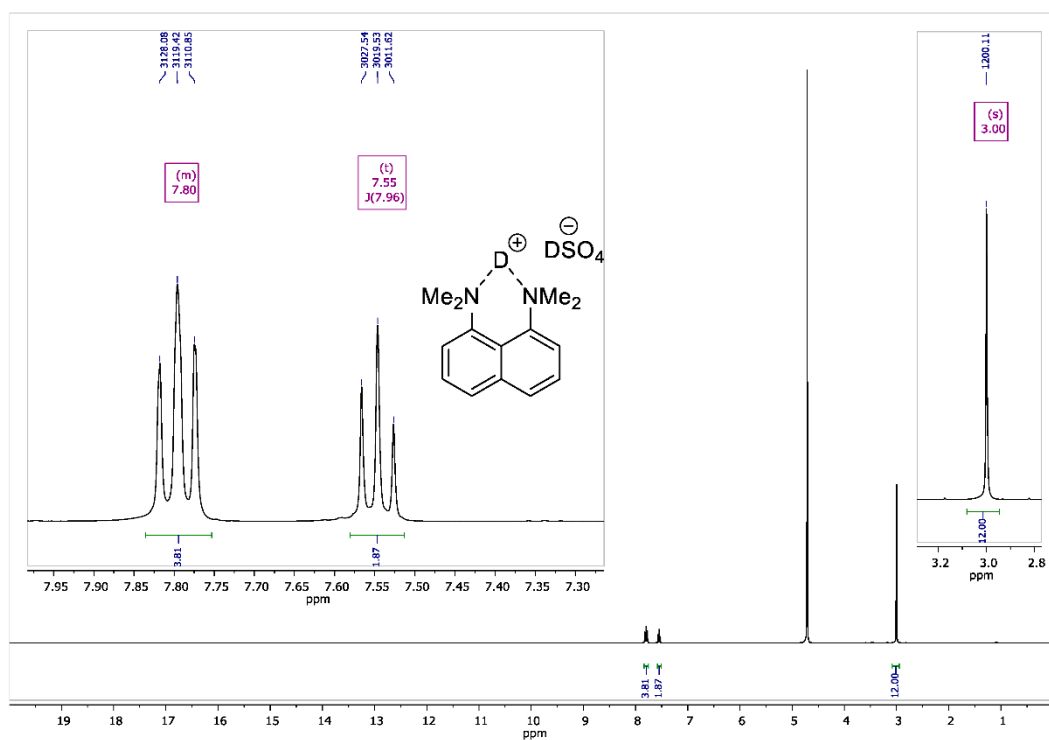


Figure A5. ^1H NMR spectrum for 1,8-bis(dimethylamino)naphthalene sulfate- d_2 (400 MHz, D_2O).

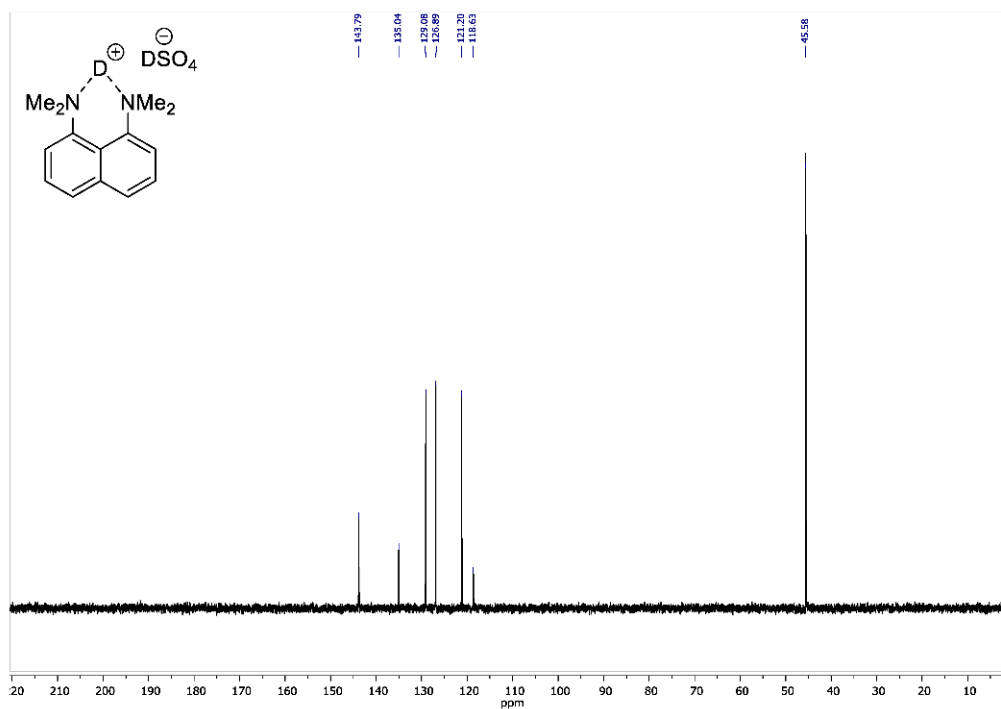


Figure A6. ^{13}C NMR spectrum for 1,8-bis(dimethylamino)naphthalene sulfate- d_2 (100 MHz, D_2O).

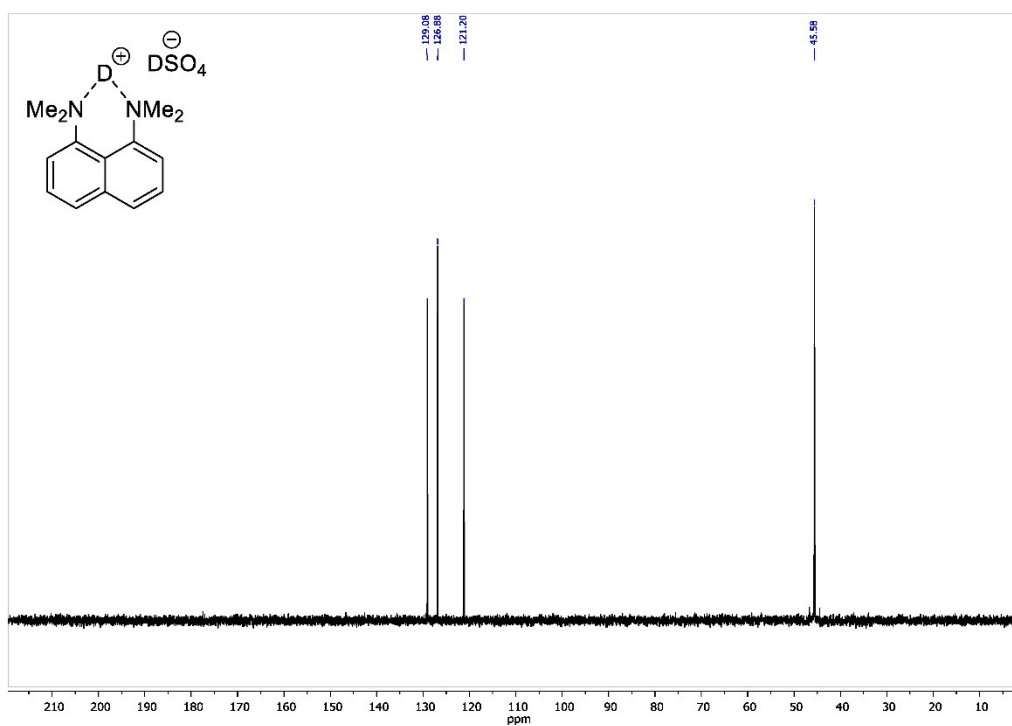


Figure A7. ^{13}C DEPT135 NMR spectrum for 1,8-bis(dimethylamino)naphthalene sulfate- d_2 (100 MHz, D_2O).

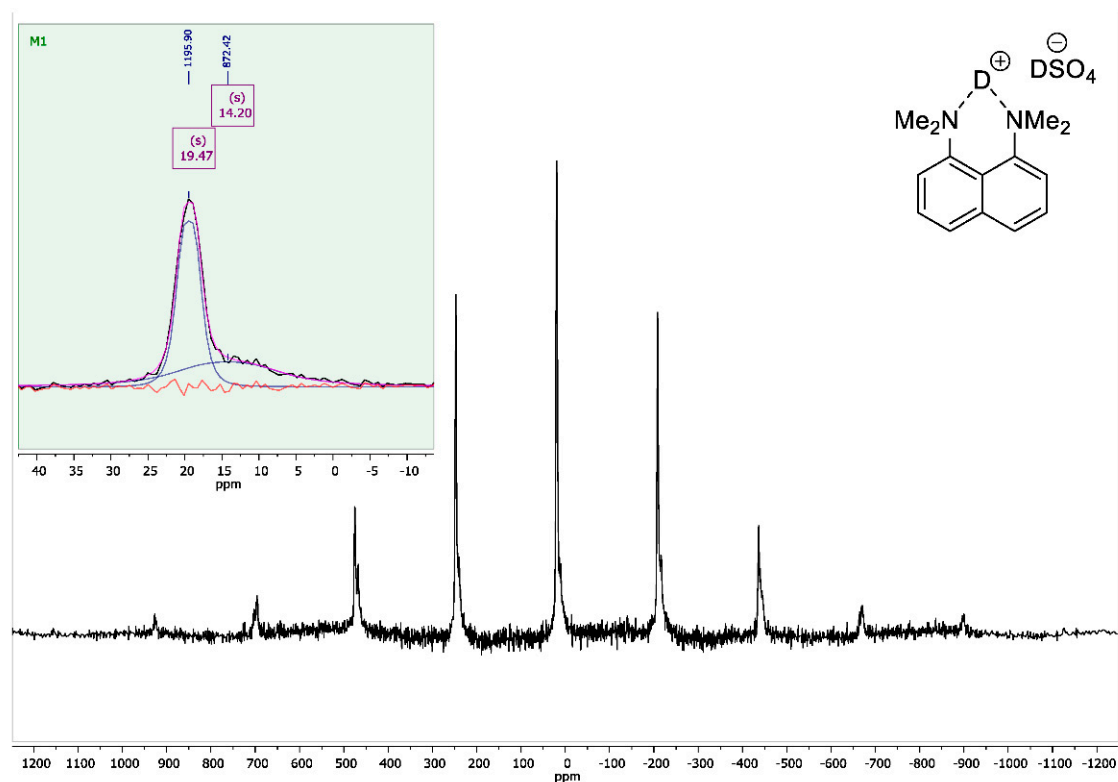


Figure A8. Solid-state ^2H NMR spectrum for 1,8-bis(dimethylamino)naphthalene sulfate- d_2 (76.7 MHz, MAS at 18 kHz).

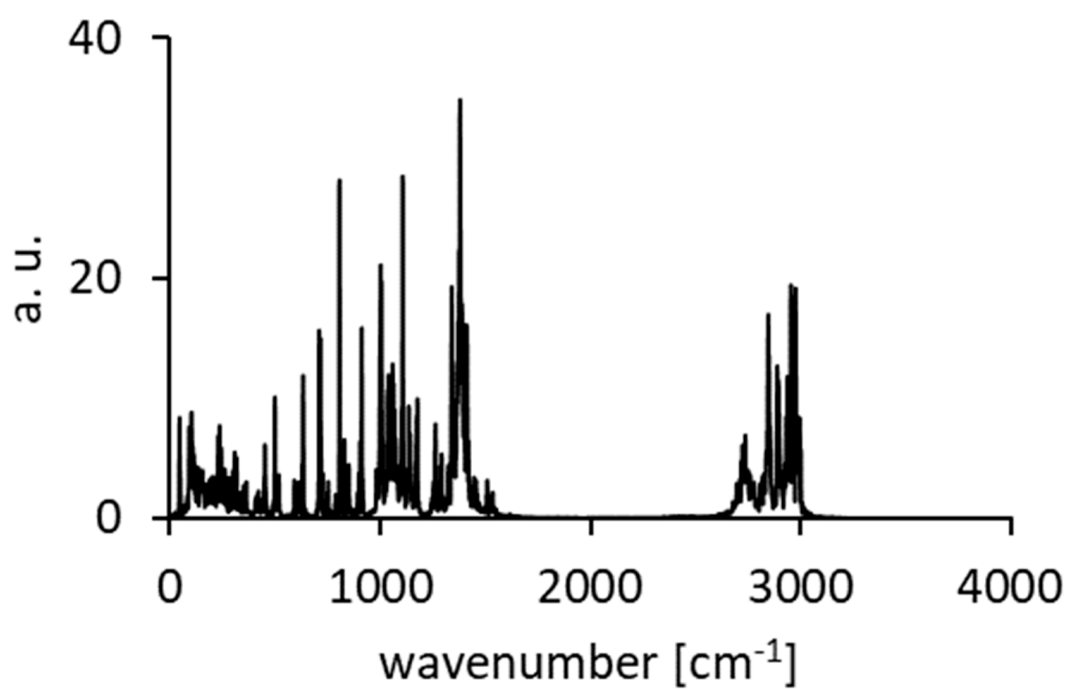


Figure A9. Calculated spectra of atomic velocity—results of the CPMD run for DMAN.

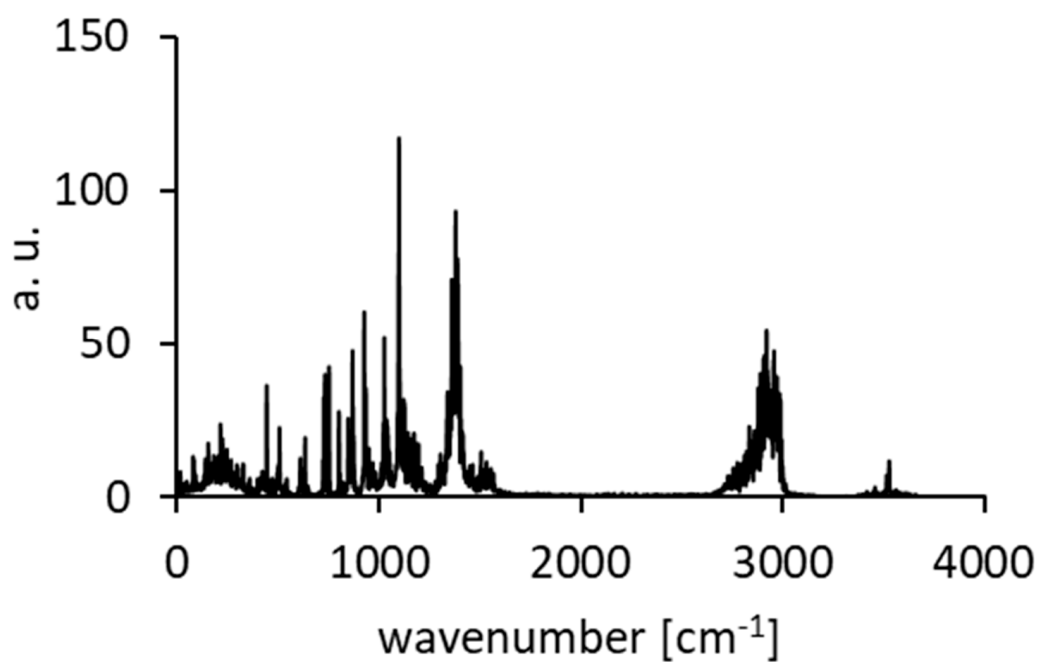


Figure A10. Calculated spectra of atomic velocity—results of the CPMD run for $\text{DMANH}^+ \text{HSO}_4^-$.

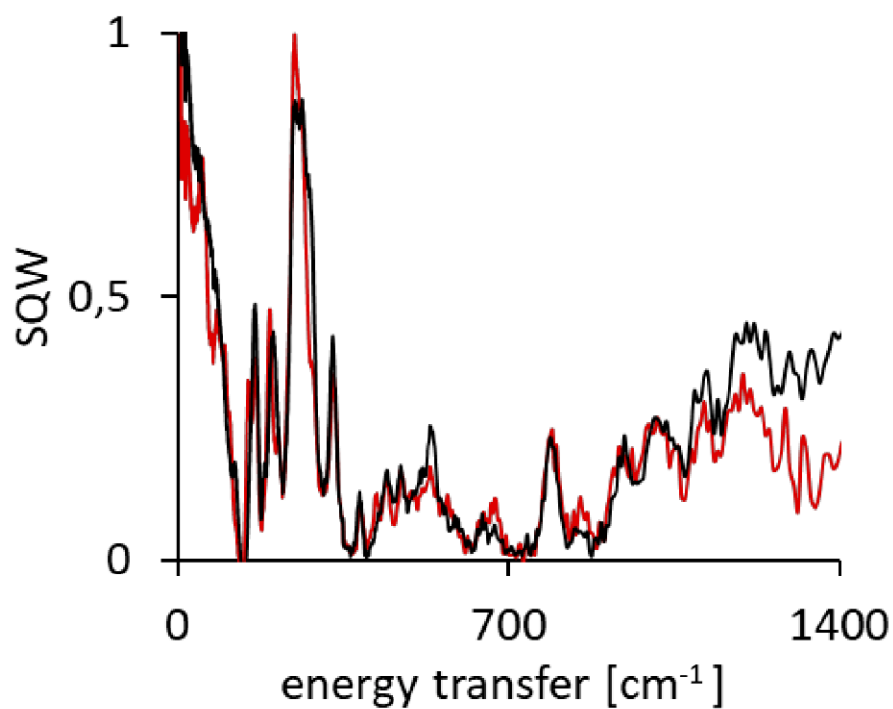


Figure A11. The IINS spectra of $\text{DMANH}^+ \text{HSO}_4^-$ (black line) and its derivative $\text{DMAND}^+ \text{DSO}_4^-$ (red line).

Table A1. Experimental IR, IINS, and calculated (B3LYP/6-311++G(d,p)) spectral data of DMAN.

Mode №	IR	IINS	Wavenumber [cm ⁻¹]	Intensities [km/mol]
	exp.	exp.	calc.	calc.
tr		9, 14, 35, 46		
1		56	51.74	0.52
2		72		
3	84	80		
4	93	91	99.49	0.23
5			115.46	3.64
6	124	122	122.23	0.28
7			126.25	1.04
8	135	141	151.23	0.59
9	162	163	172.50	0.95
10	193	190		
11		200	211.02	0.02
12	243	222	231.19	0.68
13	263	259	261.03	4.05
14	286	277	295.65	1.52
15	304	296	303.45	1.05
16		310	312.48	4.87
17		334	325.28	0.29
18	351	351	350.55	1.38
19	363	361	367.12	4.21
20	382	385	385.57	3.15
21	443	446	442.71	1.12
22	468	474	478.21	5.77
23			484.85	2.56
24	525	528	535.68	5.75
25			536.21	1.67
26			538.78	0.01
27		577	551.01	1.67
28	643	620	632.15	2.95
29	661	649	654.22	8.74
30			677.28	7.42
31	752	766	766.11	0.11
32	779		771.44	0.69
33			775.50	79.16
34			793.09	3.25
35	818		839.55	27.81
36		870	876.68	0.14
37	887		892.78	1.88
38			897.72	2.49
39	937		947.92	40.51
40	956	971	973.02	0.65
41			980.44	0.31
42	1032		1041.07	95.25
43	1056		1053.03	25.44
44			1072.89	23.97
45	1092		1073.11	9.06
46			1108.97	12.30
47	1113		1112.14	4.67
48			1122.56	0.38
49	1136		1131.23	4.10
50	1152		1158.87	0.66
51			1162.50	44.36
52	1185		1178.07	1.90

Table A1. Cont.

Mode №	IR	IINS	Wavenumber [cm ⁻¹]	Intensities [km/mol]
	exp.	exp.	calc.	calc.
53	1197		1188.05	2.11
54		1200 b	1205.20	27.08
55			1220.59	6.34
56	1226		1224.03	4.29
57			1242.37	18.36
58			1248.75	14.89
59	1324		1333.17	15.30
60	1343		1348.38	47.07
61			1360.88	23.49
62	1384		1369.77	22.02
63	1420		1407.98	74.73
64	1448		1443.03	0.43
65			1443.45	0.39
66			1456.69	21.91
67	1463	1466 b	1464.24	5.54
68			1473.32	1.03
69	1479		1477.99	0.62
70			1481.23	3.35
71			1485.18	9.10
72			1492.70	20.46
73			1493.08	30.41
74			1500.92	2.48
75	1511		1502.60	16.87
76			1521.37	11.25
77			1524.98	22.79
78	1576		1542.86	22.63
79	1605		1608.92	191.50
80	1722		1632.70	1.17
81			1641.10	11.45
82			2926.35	160.99
83	2777		2926.67	11.27
84	2824		2939.86	267.58
85	2852		2941.71	37.29
86	2928		3051.65	27.31
87	2971		3051.81	17.97
88	3013		3056.51	12.52
89	3048		3057.11	96.53
90	3093		3101.58	16.29
91			3101.61	24.04
92			3158.93	4.96
93			3159.18	17.51
94			3159.31	0.06
95			3161.34	1.11
96			3176.94	10.44
97			3180.00	43.23
98			3204.39	11.51
99			3204.41	8.22

Table A2. Experimental IR, IINS, Raman, and calculated (B3LYP/6-311++G(d,p)) spectral data of DMANH⁺ HSO₄⁻.

№	IR	IINS	Raman	Wavenumber [cm ⁻¹]	Intensities [km/mol]
	exp.	exp.	exp.	calc.	calc.
1				14.57	0.03
2				17.59	1.10
3				36.81	1.37
4				42.72	0.88
5				60.97	1.86
6				83.84	25.22
7	90			90.41	5.08
8				93.29	0.17
9				147.02	43.61
10				152.75	31.05
11		162		161.14	3.03
12		185		185.56	9.32
13				185.81	15.51
14	194	198		198.61	0.12
15				242.02	3.42
16				243.48	2.73
17		249		252.75	10.81
18				256.74	0.23
19		262	262	263.71	0.50
20		274		288.84	3.22
21		325		325.96	0.01
22			329	332.45	8.04
23				378.53	3.30
24	382	383		384.15	6.38
25				399.35	13.15
26	419			422.01	12.28
27		440	439	441.72	3.17
28	466	470		481.60	0.24
29			503	498.35	10.20
30		511		525.17	5.77
31				525.65	52.86
32	533	533	534	536.22	9.97
33				539.01	0.17
34				540.81	3.02
35				545.32	31.75
36	584	585	593	583.61	12.63
37		642		649.80	0.00
38		676		674.12	35.07
39			687	678.86	0.26
40				732.25	299.92
41				776.12	0.93
42	779			781.77	1.30
43		787		789.15	71.35
44				796.76	0.78
45	841		844	853.32	15.88
46	846		877	866.23	13.02
47				908.56	22.33
48				922.62	0.27
49		949		938.58	1.60
50				989.33	3.63
51				995.53	4.04
52				1002.12	1.26
53				1004.20	115.91
54	1007	1013	1007	1004.66	102.37
55	1031		1025	1047.32	17.60
56	1049		1049	1047.85	18.21
57			1087	1088.53	0.09
58	1099			1104.66	212.72
59				1108.80	8.72

Table A2. Cont.

№	IR	IINS	Raman	Wavenumber [cm ⁻¹]	Intensities [km/mol]
	exp.	exp.	exp.	calc.	calc.
60		1112		1110.39	10.96
61			1114	1114.95	4.13
62			1155	1170.56	30.47
63			1173	1175.17	65.76
64				1181.23	21.65
65	1193			1195.65	20.18
66				1196.71	26.24
67				1199.61	175.54
68				1200.30	166.15
69		1210		1217.08	170.92
70	1223			1228.08	9.32
71				1239.64	13.43
72				1245.05	26.67
73				1264.43	4.50
74				1305.30	11.88
75				1354.70	48.76
76			1365	1365.64	3.30
77	1379			1386.47	15.33
78	1414		1415	1436.10	1.65
79			1431	1438.56	79.01
80			1443	1451.21	3.09
81	1469			1465.77	1.48
82				1480.31	7.45
83				1482.26	0.71
84				1488.20	15.25
85				1488.98	0.97
86			1490	1497.56	0.69
87			1495	1498.85	20.69
88				1503.20	8.53
89				1505.92	5.75
90				1511.50	82.43
91	1518			1514.96	23.30
92				1521.21	24.25
93	1578		1580	1551.47	22.12
94	1603			1612.85	5.43
95	1626		1627	1617.33	8.56
96				1644.36	9.08
97				1664.89	16.75
98	2600			2529.78	977.93
99			2809	2984.75	30.16
100	2940		2866	2989.37	66.45
101			2952	3056.91	10.25
102			3015	3060.71	59.04
103			3065	3081.84	19.34
104				3082.70	19.25
105				3134.13	0.65
106				3137.65	8.34
107				3148.81	1.78
108				3150.19	9.61
109				3154.58	2.99
110				3160.22	69.10
111				3168.92	0.48
112				3172.93	0.06
113				3181.07	9.40
114				3186.35	13.84
115				3192.70	10.19
116				3198.99	4.40
117				3794.06	87.38

References

1. Perrin, C.L. Symmetries of hydrogen bonds in solution. *Science* **1994**, *266*, 1665. [[CrossRef](#)] [[PubMed](#)]
2. Perrin, C.L.; Nielson, J.B. Asymmetry of Hydrogen Bonds in Solutions of Monoanions of Dicarboxylic Acids. *J. Am. Chem. Soc.* **1997**, *119*, 12734–12741. [[CrossRef](#)]
3. Chambron, J.-C.; Meyer, M. The ins and outs of proton complexation. *Chem. Soc. Rev.* **2009**, *38*, 1663–1673. [[CrossRef](#)] [[PubMed](#)]
4. Mavri, J.; Hodošček, M.; Hadži, D. Ab initio SCF and Møller-Plesset calculations on the hydrogen bond in hydrogen malonate: Effects of neighbour ions and polarizable medium. *J. Mol. Struct.* **1990**, *209*, 421–431. [[CrossRef](#)]
5. Mavri, J.; Hadži, D. Influence of solvation on the hydrogen bond in hydrogen malonate an ab initio and semiempirical study. *J. Mol. Struct. THEOCHEM* **1998**, *432*, 257–262. [[CrossRef](#)]
6. Staab, H.A.; Kriege, C.; Hieber, G.; Oberdorf, K. 1,8-Bis(dimethylamino)4,5-dihydroxynaphthalene, a Natural, Intramolecularly Protonated “Proton Sponge” with Zwitterionic Structure. *Angew. Chem. Int. Ed. Engl.* **1997**, *36*, 1884–1886. [[CrossRef](#)]
7. Perrin, C.L.; Thoburn, J.D. Symmetries of hydrogen bonds in monoanions of dicarboxylic acids. *J. Am. Chem. Soc.* **1992**, *114*, 8559–8565. [[CrossRef](#)]
8. Perrin, C.L.; Kim, Y.J. Symmetry of the Hydrogen Bond in Malonaldehyde Enol in Solution. *J. Am. Chem. Soc.* **1998**, *120*, 12641–12645. [[CrossRef](#)]
9. Guo, J.; Tolstoy, P.M.; Koeppe, B.; Denisov, G.S.; Limbach, H.-H. NMR Study of Conformational Exchange and Geometries of Intramolecular Hydrogen Bonds in Monoanions of Succinic Acid and Derivatives. *J. Phys. Chem. A* **2011**, *115*, 9828–9836. [[CrossRef](#)]
10. Guo, J.; Tolstoy, P.M.; Koeppe, B.; Golubev, N.S.; Denisov, G.S.; Smirnov, S.N.; Limbach, H.-H. Hydrogen Bond Geometries and Proton Tautomerism of Homo-Conjugated Anions of Carboxylic Acids Studied via H/D Isotope Effects on ¹³C NMR Chemical Shifts. *J. Phys. Chem. A* **2012**, *116*, 11180–11188. [[CrossRef](#)]
11. Chmielewski, P.; Ozeryanskii, V.A.; Sobczyk, L.; Pozharskii, A.F. Primary 1 H/2 H isotope effect in the NMR chemical shift of HClO₄ salts of 1,8-bis(dimethylamino)naphthalene derivatives. *J. Phys. Org. Chem.* **2007**, *20*, 643–648. [[CrossRef](#)]
12. Zhou, S.; Wang, L. Symmetry and 1 H NMR chemical shifts of short hydrogen bonds: Impact of electronic and nuclear quantum effects. *Phys. Chem. Chem. Phys.* **2020**, *22*, 4884–4895. [[CrossRef](#)] [[PubMed](#)]
13. White, P.B.; Hong, M. 15N and 1 H Solid-State NMR Investigation of a Canonical Low-Barrier Hydrogen-Bond Compound: 1,8-Bis(dimethylamino)naphthalene. *J. Phys. Chem. B* **2015**, *119*, 11581–11589. [[CrossRef](#)] [[PubMed](#)]
14. Perrin, C.L.; Ohta, B.K. Symmetry of N–H–N Hydrogen Bonds in 1,8-Bis(dimethylamino)naphthalene-H⁺ and 2,7-Dimethoxy-1,8-bis(dimethylamino)naphthalene-H⁺. *J. Am. Chem. Soc.* **2001**, *123*, 6520–6526. [[CrossRef](#)] [[PubMed](#)]
15. Woźniak, K.; Wilson, C.C.; Knight, K.S.; Jones, W.; Grech, E. Neutron Diffraction of a Complex of 1,8-Bis(dimethylamino)naphthalene with 1,2-Dichloromaleic Acid. *Acta Cryst. B* **1996**, *52*, 691–696. [[CrossRef](#)]
16. Jones, A.O.F.; Kallay, A.A.; Lloyd, H.; McIntyre, G.J.; Wilson, C.C.; Thomas, L.H. The Effect of Local Crystalline Environment on Hydrogen Atom Behavior in Molecular Complexes of a Proton Sponge. *Cryst. Growth Des.* **2016**, *16*, 2123–2129. [[CrossRef](#)]
17. Gregorovic, A.; Apih, T.; Zagara, V.; Seliger, J. 14N NQR spectroscopy reveals the proton position in N–H N bonds: A case study with proton sponges. *Phys. Chem. Chem. Phys.* **2019**, *21*, 306–313. [[CrossRef](#)]
18. Sabet-Sarvestani, H.; Izadyar, M.; Eshghi, H.; Noroozi-Shad, N.; Bakavoli, M. Proton sponge as a new efficient catalyst for carbon dioxide transformation to methanol: Theoretical approach. *Fuel* **2018**, *221*, 491–500. [[CrossRef](#)]
19. Pawlukoć, A.; Natkaniec, I.; Grech, E.; Baran, J.; Malarski, Z.; Sobczyk, L. Incoherent inelastic neutron scattering, Raman and IR absorption studies on 1,8-bis(dimethylamino)naphthalene and its protonated forms. *Spectrochim. Acta A* **1998**, *54*, 439–448. [[CrossRef](#)]
20. Brzeziński, B.; Głowiak, T.; Grech, E.; Malarski, Z.; Sobczyk, L. Structure and IR spectra of protonated 1,8-bis(dimethylamino)naphthalene proton sponge. *Croat. Chem. Acta* **1992**, *65*, 101–108.
21. Lee, J.; Cheong, I.; Lee, S.-Y. Successful application of a neutral organic base, 1,8-bis(tetramethylguanidino)naphthalene (TMGN), for the radiosynthesis of [¹¹C]raclopride. *Appl. Rad. Isotop.* **2016**, *118*, 382–388. [[CrossRef](#)] [[PubMed](#)]

22. Lopez, C.; Lorente, P.; Claramunt, R.M.; Marin, J.; Foces-Foces, C.; Llamas-Saiz, A.L.; Elguero, J.; Limbach, H.H. Localization of Hydrogen Bond Deuterons in Proton Sponges by Dipolar Solid State N-15 NMR Spectroscopy. *Ber. Bunsenges. Phys. Chem. Chem. Phys.* **1998**, *102*, 414–418. [[CrossRef](#)]
23. Pietrzak, M.; Wehling, J.P.; Kong, S.; Tolstoy, P.M.; Shenderovich, I.G.; Lopez, C.; Claramunt, R.M.; Elguero, J.; Denisov, G.S.; Limbach, H.-H. Symmetrization of Cationic Hydrogen Bridges of Protonated Sponges Induced by Solvent and Counteranion Interactions as Revealed by NMR Spectroscopy. *Chem. Eur. J.* **2010**, *16*, 1679–1690. [[CrossRef](#)] [[PubMed](#)]
24. Pietrzak, M.; Wehling, J.; Limbach, H.-H.; Golubev, N.S.; Lopez, C.; Claramunt, R.M.; Elguero, J. ¹³C Detected Scalar Nitrogen-Nitrogen Couplings Across the Intramolecular Symmetric NHN Hydrogen Bond of Proton Sponge. *J. Am. Chem. Soc.* **2001**, *123*, 4338–4339. [[CrossRef](#)] [[PubMed](#)]
25. Lopez, C.; Claramunt, R.M.; Llamas-Saiz, A.L.; Foces-Foces, C.; Elguero, J.; Sobrados, I.; Aguilar-Parrilla, F.; Limbach, H.H. X-ray diffraction and solid state NMR studies of 1,8-bis(dimethylamino)naphthalene and its complexes with picric and hexafluorophosphoric acids. *New J. Chem.* **1996**, *20*, 523–536.
26. Saunders, M.; Telkowski, L.; Kates, M.R. NMR isotope shifts as a probe of electronic structure. *J. Am. Chem. Soc.* **1977**, *99*, 8070–8071. [[CrossRef](#)]
27. Alder, R.W.; Bowman, P.S.; Steele, W.R.S.; Winterman, D.R. The remarkable basicity of 1,8-bis(dimethylamino)naphthalene. *J. Chem. Soc. Chem. Commun.* **1968**, 723–724. [[CrossRef](#)]
28. Alder, R.W.; East, S.P. In/Out Isomerism. *Chem. Rev.* **1996**, *96*, 2097–2111. [[CrossRef](#)]
29. Staab, H.A.; Saupe, T. “Proton Sponges” and the Geometry of Hydrogen Bonds: Aromatic Nitrogen Bases with Exceptional Basicities. *Angew. Chem. Int. Ed. Engl.* **1988**, *27*, 865–879. [[CrossRef](#)]
30. Pozharskii, A.F. Naphthalene “Proton Sponges”. *Russ. Chem. Rev.* **1998**, *67*, 1–27. [[CrossRef](#)]
31. Pozharskii, A.F.; Ozeryanskii, V.A. Proton sponges. In *The Chemistry of Anilines*; Rappoport, Z., Ed.; J. Wiley & Sons: Chichester, UK, 2007; pp. 931–1026.
32. Sobczyk, L. The specificity of the [NHN]⁺ hydrogen bonds in protonated naphthalene proton sponges. *J. Mol. Struct.* **2010**, *972*, 59–63. [[CrossRef](#)]
33. Llamas-Saiz, A.L.; Foces-Foces, C.; Elguero, J. Proton sponges. *J. Mol. Struct.* **1994**, *328*, 297–323. [[CrossRef](#)]
34. Kaljurand, I.; Saame, J.; Rodima, T.; Koppel, I.; Koppel, I.A.; Kögel, J.F.; Sundermeyer, J.; Köhn, U.; Coles, M.P.; Leito, I. Experimental Basicities of Phosphazene, Guanidinophosphazene, and Proton Sponge Superbases in the Gas Phase and Solution. *J. Phys. Chem. A* **2016**, *120*, 2591–2604. [[CrossRef](#)] [[PubMed](#)]
35. Kçgel, J.F.; Xie, X.; Baal, E.; Gesevičius, D.; Oelkers, B.; Kovačević, B.; Sundermeyer, J. Superbasic Alkyl-Substituted Bisphosphazene Proton Sponges: Synthesis, Structural Features, Thermodynamic and Kinetic Basicity, Nucleophilicity and Coordination Chemistry. *Chem. Eur. J.* **2014**, *20*, 7670–7685. [[CrossRef](#)]
36. Korzhenevskaya, N.G.; Schroeder, G.; Brzezinski, B.; Rybachenko, V.I. Concept of Superbasicity of 1,8-Bis(dialkylamino)naphthalenes ([Proton Sponges]). *Rus. J. Org. Chem.* **2001**, *37*, 1603–1610. [[CrossRef](#)]
37. Raab, V.; Kipke, J.; Gschwind, R.M.; Sundermeyer, J. 1,8-Bis(tetramethylguanidino)naphthalene (TMGN): A New, Superbasic and Kinetically Active “Proton Sponge”. *Chem. Eur. J.* **2002**, *8*, 1682–1693. [[CrossRef](#)]
38. Hibbert, F.; Robbins, H.J. Base-catalyzed proton transfer from an intramolecularly hydrogen-bonded naphthylammonium ion in 70% dimethyl sulfoxide-water (v/v). *J. Am. Chem. Soc.* **1978**, *100*, 8239–8244. [[CrossRef](#)]
39. Hibbert, F.; Simpson, G.R. Acid–base properties of highly substituted diamionaphthalenes. *J. Chem. Soc. Perkin Trans.* **1987**, *2*, 243–246. [[CrossRef](#)]
40. Woźniak, K.; He, H.Y.; Klinowski, J.; Barr, T.L.; Milart, P. ESCA and Solid-State NMR Studies of Ionic Complexes of 1,8-Bis(dimethylamino)naphthalene. *J. Phys. Chem.* **1996**, *100*, 11420–11426. [[CrossRef](#)]
41. Parkin, A.; Woźniak, K.; Wilson, C.C. From Proton Disorder to Proton Migration: A Continuum in the Hydrogen Bond of a Proton Sponge in the Solid State. *Cryst. Grow. Des.* **2007**, *7*, 1393–1398. [[CrossRef](#)]
42. Hoser, A.A.; Dobrzycki, Ł.; Gutmann, M.J.; Woźniak, K. Charge Densities of Two Polymorphs of Hydrated 1,8-Bis(dimethylamino)naphthalene Hydrochloride; Similarities and Differences. *Cryst. Grow. Des.* **2010**, *10*, 5092–5104. [[CrossRef](#)]
43. Mallinson, P.R.; Smith, G.T.; Wilson, C.C.; Grech, E.; Wozniak, K. From Weak Interactions to Covalent Bonds: A Continuum in the Complexes of 1,8-Bis(dimethylamino)naphthalene. *J. Am. Chem. Soc.* **2003**, *125*, 4259–4270. [[CrossRef](#)] [[PubMed](#)]

44. Woźniak, K.; Krygowski, T.M.; Kariuki, B.; Jones, W.; Grech, E. Crystallographic Studies on Sterically Affected Chemical-Species 0.2. Molecular and Crystal-Structure of 1,8-Bis(Dimethylamino)-Naphthalene Tetrafluoroborate—Analysis of Distortion of Geometry in the Aromatic Part Due to Intramolecular Hydrogen-Bonding. *J. Mol. Struct.* **1990**, *240*, 111–118. [[CrossRef](#)]
45. Grech, E.; Klimkiewicz, J.; Nowicka-Scheibe, J.; Pietrzak, M.; Schilf, W.; Pozharski, A.F.; Ozeryanskii, V.A.; Bolvig, S.; Abildgaard, J.; Hansen, P.E. Deuterium isotope effects on ¹⁵N, ¹³C and ¹H chemical shifts of proton sponges. *J. Mol. Struct.* **2002**, *615*, 121–140. [[CrossRef](#)]
46. Pawełka, Z.; Zeegers-Huyskens, T. The strange behaviour of the hydrogen bond complexes of 1,8-bis(dimethylamino) naphthalene in solution. *J. Mol. Struct. THEOCHEM* **1989**, *200*, 565–573. [[CrossRef](#)]
47. Ozeryanskii, V.A.; Pozharski, A.F.; Bieńko, A.J.; Sawka-Dobrowolska, W.; Sobczyk, L. [NHN]⁺ Hydrogen Bonding in Protonated 1,8-Bis(dimethylamino)-2,7-dimethoxynaphthalene. X-ray Diffraction, Infrared, and Theoretical ab Initio and DFT Studies. *J. Phys. Chem. A* **2005**, *109*, 1637–1642. [[CrossRef](#)]
48. Ozeryanskii, V.A.; Pozharski, A.F.; Głowiak, T.; Majerz, I.; Sobczyk, L.; Grech, I.; Nowicka-Szajbe, J. X-ray diffraction and IR-spectroscopic studies on protonated 4-amino-1,8-bis(dimethylamino)naphthalene. *J. Mol. Struct.* **2002**, *607*, 1–8. [[CrossRef](#)]
49. Brzezinski, B.; Schroeder, G.; Jarczewski, A.; Grech, E.; Nowicka-Scheibe, J.; Stefaniak, L.; Klimkiewicz, J. Proton transfer reactions from N-H acid to proton sponges in acetonitrile. Part 2. *J. Mol. Struct.* **1996**, *377*, 149–154.
50. Baran, J.; Pawlukojc, A.; Majerz, I.; Malarski, Z.; Sobczyk, L.; Grech, E. Vibrational spectra of the adduct of 1,8-bis(dimethylamino)naphthalene with dichloromaleic acid (DMAN*DCM). *Spectrochim. Acta A* **2000**, *56*, 1801–1812. [[CrossRef](#)]
51. Belding, L.; Stoyanov, P.; Dudding, T. Synthesis, Theoretical Analysis, and Experimental pKa Determination of a Fluorescent, Nonsymmetric, In–Out Proton Sponge. *J. Org. Chem.* **2016**, *81*, 6–13. [[CrossRef](#)]
52. Antonov, A.S.; Pozharski, A.F.; Tolstoy, P.M.; Filarowski, A.; Khoroshilova, O.V. 1,8-Bis(dimethylamino) naphthyl-2-ketimines: Inside vs outside protonation. *Beilstein J. Org. Chem.* **2018**, *14*, 2940–2948. [[CrossRef](#)] [[PubMed](#)]
53. Ozeryanskii, V.A.; Pozharski, A.F.; Antonov, A.S.; Filarowski, A. Out-Basicity of 1,8-bis(dimethylamino) naphthalene: The experimental and theoretical challenge. *Org. Biomol. Chem.* **2014**, *12*, 2360–2369. [[CrossRef](#)] [[PubMed](#)]
54. Pozharski, A.F.; Degtyarev, A.V.; Ryabtsova, O.V.; Ozeryanskii, V.A.; Kletskii, M.E.; Starikova, Z.A.; Sobczyk, L.; Filarowski, A. 2- α -hydroxyalkyl- and 2,7-di(α -hydroxyalkyl)-1,8-bis(dimethylamino)naphthalenes: Stabilization of nonconventional in/out conformers of “proton sponges” via N \cdots H-O intramolecular hydrogen bonding. A remarkable kind of tandem nitrogen inversion. *J. Org. Chem.* **2007**, *72*, 3006–3019. [[CrossRef](#)] [[PubMed](#)]
55. Belding, L.; Dudding, T. Synthesis and Theoretical Investigation of a 1,8-Bis(bis(diisopropylamino) cyclopropeniminyl)naphthalene Proton Sponge Derivative. *Chem. Eur. J.* **2014**, *20*, 1032–1037. [[CrossRef](#)] [[PubMed](#)]
56. Jezierska, A.; Panek, J.J. Theoretical study of intramolecular hydrogen bond in selected symmetric “proton sponges” on the basis of DFT and CPMD methods. *J. Mol. Model.* **2020**, *26*, 37. [[CrossRef](#)]
57. Jezierska, A.; Panek, J.J. “Zwitterionic proton sponge” hydrogen bonding investigations on the basis of Car-Parrinello molecular dynamics. *J. Chem. Inf. Model.* **2015**, *55*, 1148–1157. [[CrossRef](#)]
58. Masuda, Y.; Mori, Y.; Sakurai, K. Effects of Counterion and Solvent on Proton Location and Proton Transfer Dynamics of N–H \cdots N Hydrogen Bond of Monoprotonated 1,8-Bis(dimethylamino)naphthalene. *J. Phys. Chem. A* **2013**, *117*, 10576–10587. [[CrossRef](#)]
59. Majerz, I.; Olovsson, I. Proton transfer in the intramolecular NHN⁺ bonds in proton sponges with different hydrogen bridge flexibility. *Phys. Chem. Chem. Phys.* **2009**, *11*, 1297–1302. [[CrossRef](#)]
60. Majerz, I.; Olovsson, I. The shape of the potential energy curves for NHN⁺ hydrogen bonds and the influence of non-linearity. *Phys. Chem. Chem. Phys.* **2008**, *10*, 3043–3051. [[CrossRef](#)]
61. Horbatenko, Y.; Vyboishchikov, S.F. Hydrogen Motion in Proton Sponge Cations: A Theoretical Study. *ChemPhysChem* **2011**, *12*, 1118–1129. [[CrossRef](#)]
62. Pozharski, A.F.; Ryabtsova, O.V.; Ozeryanskii, V.A.; Degtyarev, A.V.; Kazheva, O.N.; Alexandrov, G.G.; Dyachenko, O.A. Organometallic Synthesis, Molecular Structure, and Coloration of 2,7-Disubstituted 1,8-Bis(dimethylamino)naphthalenes. How Significant Is the Influence of “Buttressing Effect” on Their Basicity? *J. Org. Chem.* **2003**, *68*, 10109–10122. [[CrossRef](#)]

63. Alder, R.W.; Orpen, A.G.; Sessions, R.B. The structure of 1,6-diazabicyclo[4.4.4]tetradecane and of its inside protonated ion. *J. Chem. Soc. Chem. Commun.* **1983**, 999–1000. [[CrossRef](#)]
64. Alder, R.W.; Bryce, M.R.; Goode, N.C.; Miller, N.; Owen, J. Preparation of a range of NNN'N'-tetrasubstituted 1,8-diaminonaphthalenes. *J. Chem. Soc. Perkin Trans.* **1981**, 1, 2840–2847. [[CrossRef](#)]
65. Degtyarev, A.V.; Ryabtsova, O.V.; Pozharskii, A.F.; Ozeryanskii, V.A.; Starikova, Z.A.; Sobczyk, L.; Filarowski, A. 2,7-disubstituted proton sponges as borderline systems for investigating barrier-free intramolecular hydrogen bonds. Protonated 2,7-bis(trimethylsilyl)- and 2,7-di(hydroxymethyl)-1,8-bis(dimethylamino)naphthalenes. *Tetrahedron* **2008**, 64, 6209–6214. [[CrossRef](#)]
66. Pozharskii, A.F.; Ozeryanskii, V.A.; Starikova, Z.A. Molecular structure of 5,6-bis(dimethylamino)acenaphthene, 5,6-bis(dimethylamino)acenaphthylene, and their monohydrobromides: A comparison with some naphthalene proton sponges. *J. Chem. Soc. Perkin Trans.* **2002**, 2, 318–322. [[CrossRef](#)]
67. Barnett, G.H.; Hibbert, F. General base catalysis, isotope effects, activation parameters, and the mechanism of removal of the hydrogen-bonded proton from protonated 1,8-bis(diethylamino)-2,7-dimethoxynaphthalene. *J. Am. Chem. Soc.* **1984**, 106, 2080–2084. [[CrossRef](#)]
68. Filatova, E.A.; Gulevskaya, A.V.; Pozharskii, A.F.; Ermolenko, E.A.; Ozeryanskii, V.A.; Misharev, A.D. Synthesis of 2-Aryl- and 2,7-Diaryl-1,8-bis(dimethylamino)naphthalenes. Overview of the “Buttressing effect” in 2,7-Disubstituted Proton Sponges. *ChemistrySelect* **2020**, 5, 9932–9945. [[CrossRef](#)]
69. Randolph, C.E.; Fabijanczuk, K.C.; Blanksby, S.J.; McLuckey, S.A. Proton Transfer Reactions for the Gas-Phase Separation, Concentration, and Identification of Cardiolipins. *Anal. Chem.* **2020**, 92, 10847–10855. [[CrossRef](#)]
70. Swor, C.D.; Zakharov, L.N.; Tyler, D.R. A Colorimetric Proton Sponge. *J. Org. Chem.* **2010**, 75, 6977–6979. [[CrossRef](#)]
71. Car, R.; Parrinello, M. Unified Approach for Molecular Dynamics and Density-Functional Theory. *Phys. Rev. Lett.* **1985**, 55, 2471–2474. [[CrossRef](#)]
72. Mitchell, P.C.H.; Parker, S.F.; Ramirez-Cuesta, A.J.; Tomkinson, J. *Series on Neutron Techniques and Applications, Vibrational Spectroscopy with Neutrons*; World Scientific Publishing Co. Pte. Ltd.: Singapore, 2005.
73. Harris, R.K.; Becker, E.D.; Cabral de Menezes, S.M.; Goodfellow, R.; Granger, P. NMR nomenclature. Nuclear spin properties and conventions for chemical shifts (IUPAC recommendations 2001). *Pure Appl. Chem.* **2001**, 73, 1795–1818. [[CrossRef](#)]
74. Mestrelab Research, S.L. Available online: <https://mestrelab.com/software/mnova> (accessed on 12 October 2020).
75. Frisch, M.J.; Trucks, G.W.; Schlegel, H.B.; Scuseria, G.E.; Robb, M.A.; Cheeseman, J.R.; Scalmani, G.; Barone, V.; Petersson, G.A.; Nakatsuji, H. *et al. Gaussian 16, Revision C.01*; Gaussian, Inc.: Wallingford, CT, USA, 2016.
76. Becke, A.D. Density-functional thermochemistry. III. The role of exact exchange. *J. Chem. Phys.* **1993**, 98, 5648–5652. [[CrossRef](#)]
77. Lee, C.; Yang, W.; Parr, R.G. Development of the Colle-Salvetti Correlation-Energy Formula into a Functional of the Electron Density. *Phys. Rev. B* **1988**, 37, 785–789. [[CrossRef](#)]
78. McLean, A.D.; Chandler, G.S. Contracted Gaussian basis sets for molecular calculations. I. Second row atoms, Z=11–18. *J. Chem. Phys.* **1980**, 72, 5639–5648. [[CrossRef](#)]
79. Krishnan, R.; Binkley, J.S.; Seeger, R.; Pople, J.A. Self-consistent molecular orbital methods. XX. A basis set for correlated wave functions. *J. Chem. Phys.* **1980**, 72, 650–654. [[CrossRef](#)]
80. Frisch, M.J.; Pople, J.A.; Binkley, J.S. Self-consistent molecular orbital methods 25. Supplementary functions for Gaussian basis sets. *J. Chem. Phys.* **1984**, 80, 3265–3269. [[CrossRef](#)]
81. Grimme, S. Semiempirical GGA-type Density Functional Constructed with a Long-Range Dispersion Correction. *J. Comput. Chem.* **2006**, 27, 1787–1799. [[CrossRef](#)]
82. Tomasi, J.; Mennucci, B.; Cammi, R. Quantum mechanical continuum solvation models. *Chem. Soc. Rev.* **2005**, 105, 2999–3093. [[CrossRef](#)]
83. Schaftenaar, G.; Noordik, J.H. Molden: A pre- and post-processing program for molecular and electronic structures. *J. Comput. Aided Mol. Design.* **2000**, 14, 123–134. [[CrossRef](#)]
84. Jeziorski, B.; Moszyński, R.; Szalewicz, K. Perturbation Theory Approach to Intermolecular Potential Energy Surfaces of van der Waals Complexes. *Chem. Rev.* **1994**, 7, 1887–1930. [[CrossRef](#)]
85. Hohenstein, E.G.; Sherrill, C.D. Density fitting of intramonomer correlation effects in symmetry-adapted perturbation theory. *J. Chem. Phys.* **2010**, 133, 014101. [[CrossRef](#)] [[PubMed](#)]
86. Kendall, R.A.; Dunning, T.H., Jr.; Harrison, R.J. Electron affinities of the first-row atoms revisited. Systematic basis sets and wave functions. *J. Chem. Phys.* **1992**, 96, 6796–6806. [[CrossRef](#)]

87. Parrish, R.M.; Burns, L.A.; Smith, D.G.A.; Simmonett, A.C.; DePrince, A.E.; Hohenstein, E.G.; Bozkaya, U.; Sokolov, A.Y.; Di Remigio, R.; Richard, R.M.; et al. Psi4 1.1: An Open-Source Electronic Structure Program Emphasizing Automation, Advanced Libraries, and Interoperability. *J. Chem. Theory Comput.* **2017**, *13*, 3185–3197. [[CrossRef](#)]
88. CPMD 3.17.1; IBM Corp: 1990–2004; MPI für Festkörperforschung Stuttgart, 1997–2001.
89. Humphrey, W.; Dalke, A.; Schulten, K. VMD—Visual Molecular Dynamics. *J. Mol. Graph.* **1996**, *14*, 33–38. [[CrossRef](#)]
90. Gnuplot 4.2; Thomas Williams, Colin Kelley, 1986–1993, 1998, 2004, 2007.
91. Perdew, J.P.; Burke, K.; Ernzerhof, M. Generalized Gradient Approximation Made Simple. *Phys. Rev. Lett.* **1996**, *77*, 3865–3868. [[CrossRef](#)]
92. Troullier, N.; Martins, J.L. Efficient pseudopotentials for plane-wave calculations. *Phys. Rev.* **1991**, *B43*, 1993–2006. [[CrossRef](#)]
93. Hockney, R.W. The potential calculation and some applications. *Meth. Comput. Phys.* **1970**, *9*, 136–211.
94. Nosé, S. A unified formulation of the constant temperature molecular dynamics methods. *J. Chem. Phys.* **1984**, *81*, 511–519. [[CrossRef](#)]
95. Hoover, W.G. Canonical dynamics: Equilibrium phase-space distributions. *Phys. Rev.* **1985**, *A31*, 1695–1697. [[CrossRef](#)]
96. Grimme, S.; Hansen, A.; Brandenburg, J.G.; Bannwarth, C. Dispersion-Corrected Mean-Field Electronic Structure Methods. *Chem. Rev.* **2016**, *116*, 5105–5154. [[CrossRef](#)]
97. Herschlag, D.; Pinney, M.M. Hydrogen Bonds: Simple after All? *Biochemistry* **2018**, *57*, 3338–3352. [[CrossRef](#)] [[PubMed](#)]
98. Sigala, P.A.; Ruben, E.A.; Liu, C.W.; Piccoli, P.M.B.; Hohenstein, E.G.; Martínez, T.J.; Schultz, A.J.; Herschlag, D. Determination of hydrogen bond structure in water versus aprotic environments to test the relationship between length and stability. *J. Am. Chem. Soc.* **2015**, *137*, 5730–5740. [[CrossRef](#)] [[PubMed](#)]
99. Ashkar, R.; Bilheux, H.Z.; Bordallo, H.; Briber, R.; Callaway, D.J.E.; Cheng, X.; Chu, X.-Q.; Curtis, J.E.; Dadmun, M.; Fenimore, P.; et al. Neutron scattering in the biological sciences: Progress and prospects. *Acta Cryst.* **2018**, *D74*, 1129–1168. [[CrossRef](#)] [[PubMed](#)]
100. Hudson, B.S. Inelastic Neutron Scattering: A Tool in Molecular Vibrational Spectroscopy and a Test of ab Initio Methods. *Phys. Chem. A* **2001**, *105*, 3949–3960. [[CrossRef](#)]
101. Hudson, B.S. Vibrational spectroscopy using inelastic neutron scattering: Overview and outlook. *Vibr. Spectr.* **2006**, *42*, 25–32. [[CrossRef](#)]
102. Pusztai, L. Neutron Scattering Methods in Chemistry. In *Handbook of Nuclear Chemistry*; Vértes, A., Nagy, S., Klencsár, Z., Lovas, R.G., Rösch, F., Eds.; Springer: Boston, MA, USA, 2011.
103. Albers, P.W.; Parker, S.W. IINS Inelastic Incoherent Neutron Scattering in Catalysis Research. *Adv. Catal.* **2007**, *51*, 99–132.
104. Tsapatsaris, N.; Kolesov, B.A.; Fischer, J.; Boldyreva, E.V.; Daemen, L.; Eckert, J.; Bordallo, H.N. Polymorphism of Paracetamol: A New Understanding of Molecular Flexibility through Local Methyl Dynamics. *Mol. Pharm.* **2014**, *11*, 1032–1041. [[CrossRef](#)] [[PubMed](#)]
105. Pawlukoć, A.; Prager, M.; Sawka-Dobrowolska, W.; Bator, G.; Sobczyk, L.; Ivanov, A.; Rols, S.; Grech, E.; Nowicka-Scheibe, J.; Unruh, T. The structure, methyl rotation reflected in elastic and quasielastic neutron scattering and vibrational spectra of 1,2,3,5-tetramethoxybenzene and its 2:1 complex with 1,2,4,5-tetracyanobenzene. *J. Chem. Phys.* **2008**, *129*, 154506–154512. [[CrossRef](#)] [[PubMed](#)]
106. Bordallo, H.N.; Zakharov, B.A.; Boldyreva, E.V.; Johnson, M.R.; Koza, M.M.; Seydel, T.; Fischer, J. Application of Incoherent Inelastic Neutron Scattering in Pharmaceutical Analysis: Relaxation Dynamics in Phenacetin. *Mol. Pharm.* **2012**, *9*, 2434–2441. [[CrossRef](#)] [[PubMed](#)]
107. Bordallo, H.N.; Barthes, M.; Eckert, J. Vibrational dynamics of crystalline L-alanine. *Phys. B* **1998**, *241*–243, 1138–1140. [[CrossRef](#)]
108. Pawlukoć, A.; Natkaniec, I.; Bator, G.; Sobczyk, L.; Grech, E.; Nowicka-Scheibe, J. Low frequency internal modes of 1,2,4,5-tetramethylbenzene, tetramethylpyrazine and tetramethyl-1,4-benzoquinone. INS, Raman, IR and theoretical DFT studies. *Spectrochim. Acta A* **2006**, *63*, 766–773. [[CrossRef](#)] [[PubMed](#)]
109. Prager, M.; Pawlukoć, A.; Wischniewski, A.; Wuttke, J. Inelastic neutron scattering study of methyl groups rotation in some methylxanthines. *J. Chem. Phys.* **2007**, *127*, 214509–214519. [[CrossRef](#)] [[PubMed](#)]

110. Bator, G.; Sawka-Dobrowolska, W.; Sobczyk, L.; Grech, E.; Nowicka-Scheibe, J.; Pawlukojs, A.; Wuttke, J.; Baran, J.; Owczarek, M. 4,4', 5,5', and 6,6'-dimethyl-2,2'-bipyridyls: The structures, phase transitions, vibrations, and methyl group tunneling of their complexes with chloranilic acid. *J. Chem. Phys.* **2011**, *135*, 044509. [[CrossRef](#)] [[PubMed](#)]
111. Singh, A.; Gangopadhyay, D.; Nandi, R.; Sharma, P.; Singh, R.K. Raman signatures of strong and weak hydrogen bonds in binary mixtures of phenol with acetonitrile, benzene and orthodichlorobenzene. *Raman Spectr.* **2016**, *47*, 712–719. [[CrossRef](#)]
112. Abe, N.; Ito, M. Effects of hydrogen bonding on the Raman intensities of methanol, ethanol and water. *Raman Spectr.* **1978**, *7*, 161–167. [[CrossRef](#)]
113. Zundel, G. *The Hydrogen Bond. Recent Developments in Theory and Experiments*; Schuster, P., Zundel, G., Sandorfy, C., Eds.; North-Holland: Amsterdam, The Netherlands, 1976; Volume 2, pp. 683–766.
114. Zundel, G. Hydrogen bonds with large proton polarizability and proton transfer processes in electrochemistry and biology. *Adv. Chem. Phys.* **2000**, *111*, 1–217.
115. Kwocz, A.; Panek, J.J.; Jezierska, A.; Hetmańczyk, Ł.; Pawlukojs, A.; Kochel, A.; Lipkowski, P.; Filarowski, A. A molecular roundabout: Triple cycle-arranged hydrogen bonds in light of experiment and theory. *New J. Chem.* **2018**, *42*, 19467–19477. [[CrossRef](#)]
116. Józwiak, K.; Jezierska, A.; Panek, J.J.; Goremychkin, E.A.; Tolstoy, P.M.; Shenderovich, I.G.; Filarowski, A. Inter- vs. intra-molecular hydrogen bond patterns and proton dynamics in phthalic acid associates. *Molecules* **2020**, *25*, 4720. [[CrossRef](#)]

Publisher's Note: MDPI stays neutral with regard to jurisdictional claims in published maps and institutional affiliations.



© 2020 by the authors. Licensee MDPI, Basel, Switzerland. This article is an open access article distributed under the terms and conditions of the Creative Commons Attribution (CC BY) license (<http://creativecommons.org/licenses/by/4.0/>).